Synthesis of Graphene Aerogel and Its Applications

by

Ecem Çelik

A Dissertation Submitted to the
Graduate School of Sciences and Engineering
in Partial Fulfillment of the Requirements for
the Degree of

Master of Science

in

Chemistry

KOÇ
ÜNİVERSİTESİ

August 31, 2020

Synthesis of Graphene Aerogel and Its Applications

Koç University

Graduate School of Sciences and Engineering

This is to certify that I have examined this copy of a master's thesis by

Ecem Çelik

and have found that it is complete and satisfactory in all respects,
and that any and all revisions required by the final
examining committee have been made.

Committee Members:

Asst. Prof. Dr. Onur Ergen (Advisor)

Assoc. Prof. Dr. Uğur Ünal

Prof. Dr. Ali Çırpan

Date: 31.08.2020

To my family

ABSTRACT

Synthesis of Graphene Aerogel and Its Applications

Ecem Çelik

Master of Science in Chemistry

August 31, 2020

Three-dimensional (3D) graphene-based aerogels with well-defined interconnected porous networks are one of the lightest materials in the world. Thanks to their excellent properties, which include large surface area, controllable porous structure and functionalizable surface properties, they have not only electronic transmission capability but also unique features of interconnected networks and can be embedded in different materials. Also, graphene aerogels (GAs) have fascinating properties such as low density, low thermal conductivity, high adsorption capacity, high mechanical strength, and electrical conductivity. Due to these features, they attract the attention of various research areas. Up to now, many synthesis methods have been used to produce GAs, which differ in performance and structure. This thesis is devoted to the synthesis of GA via one step hydrothermal treatment of graphene oxide (GO) solutions based on modified Hummer's method and the fabrication of different strain sensors based on these produced GAs for its applications. To achieve this, GO and reduced graphene oxide (rGO) solutions are synthesized as precursors to produce the high surface area GAs (~700 m^2/g) with the support of supercritical CO_2 (scCO2) drying. Obtained GAs are used to construct GA based hybrid materials for the fabrication of strain sensors as its applications.

Strain sensors are very attractive tools for structural health monitoring applications and intelligent management. Especially, flexible piezotronics strain sensors provide high sensitivity and fast response times which make them an ideal candidate for these applications. Therefore, the nanostructured architectures have become very attractive but challenging in the recent years. Various designs have been developed using different piezoelectric materials, yet most applications use ZnO nanomaterials due to their unique advantages such as biocompatibility and optical properties. However, these nanowires require a compatible host material that includes ZnO electronically and permits them a flexible movement. To satisfy this need, ZnO nanowires (ZnO-NWs) are constantly embedded in various materials to build flexible strain sensors. In this thesis, we develop a technique to produce a flexible piezotronics strain sensor based on ZnO-NWs embedded in the synthesized GA substrates, since GAs provide excellent receiving substrate properties, which in turn helps to maintain ZnO piezoelectric properties under any conditions. Moreover, this defined strain sensor is fabricated with chemical vapor deposition (CVD) grown ZnO-NWs film on the synthesized GA substrate. Strain sensing, both static and dynamic loading, is demonstrated to show that GAs are promising candidates as a host material due to their remarkable properties. Additionally, the I-V characteristic of the sensor shows high sensitivity owing to the desirable piezotronics properties, piezo potential modulated changes in Schottky barrier height (SBH), under both static and dynamic loads. A good gauge factor (GF) of as high as 120 has been demonstrated, which is almost 50 % higher than GF for any ZnO/Carbon based strain sensor.

Besides, numerous efforts are made to develop wearable devices through the utilization of nanomaterials, including nanowires, carbon nanotubes, and two-dimensional (2D) materials. Particularly, graphene has been extensively studied for wearable applications thanks to its excellent electrical and mechanical properties. Especially, the focus is on the 3D graphene-based sensor architectures such as conductive foam, nano-papers, etc. However, all geometries still confront some obstacles with conformal integration and sensitivity. Hence, a novel method to create GA based strain sensors which can effectively extract information from involuntary human motion is demonstrated in this thesis. GAs were uniquely strengthened with carbon nanotubes (CNTs) to produce 3D hybrid frameworks. These provide stretchable characteristics, which is desirable since the conductive pathways are often maintained under high strain or stress conditions. Maintaining the conductive pathways is extremely important to supply reliable information, yet it is one of the challenges in strain sensor design. However, combination of GA and CNTs provides a superb framework for reliable data gathering and their material functionalization properties provide great opportunity to supply sensitive sensors. During this study, a strain sensor was prepared from highly functionalized GA by reconstruction with CNTs and dispersing technique, which is straightforward, low cost, and scalable.

ÖZETÇE

Grafen Aerojel Sentezlenmesi ve Uygulamaları

Ecem Çelik

Kimya Bölümü, Yüksek Lisans

31 Ağustos 2020

İyi tanımlanmış, birbirine bağlı gözenekli ağlara sahip, üç boyutlu (3D) grafen bazlı aerojeller, dünyadaki en hafif malzemelerden biridir. Geniş yüzey alanı, kontrol edilebilir gözenekli yapı ve işlevselleştirilebilir yüzey alanları içeren mükemmel özellikleri sayesinde, sadece elektronik iletim kapasitesine değil, aynı zamanda birbirine bağlı ağların benzersiz özelliklerine de sahiptirler ve farklı malzemelere gömülebilirler. Ek olarak, grafen aerojeller (GA'lar) düşük yoğunluk, düşük termal iletkenlik, yüksek adsorpsiyon kapasitesi, yüksek mekanik mukavemet ve elektrik iletkenliği gibi büyüleyici özelliklere sahiptir. Bu özellikleri nedeniyle çeşitli araştırma alanlarının dikkatini çekmektedirler. Şimdiye kadar, performans ve yapı bakımından farklılık gösteren GA'ları üretmek için birçok sentez yöntemi kullanılmıştır. Bu tez, modifiye Hummer metoduna dayanan grafen oksit (GO) çözeltilerinin tek aşamalı hidrotermal muamelesi ve uygulamaları için üretilen bu GA'lara dayanan farklı gerinim sensörlerinin üretilmesi yoluyla grafen aerojel sentezine ayrılmıştır. Bu amaçla, süperkritik CO_2 ($scCO_2$) kurutma desteği ile yüksek yüzey alanı olan GA'ları (~ 700 m^2/g) üretmek için öncü olarak GO ve indirgenmiş grafen oksit (rGO) çözeltileri sentezlenmiştir. Elde edilen GA'lar, gerinim sensörlerinin uygulamaları için GA tabanlı hibrid malzemeleri oluşturmak için kullanılmıştır.

Gerinim sensörleri yapısal sağlık izleme uygulamaları ve akıllı yönetim için ilgi çeken bir materyaldir. Özellikle esnek piezotronik gerinim sensörlerinin yüksek hassasiyetleri ve hızlı tepki süreleri bu uygulamalar için onları ideal birer aday yapar. Bu alanda nanoyapılı tasarımları oluşturmak çok zorlayıcı bir hal alması nedeniyle araştırmaların ilgisini çekmektedir. Bu nedenle, birçok farklı piezoelektrik malzeme için çeşitli tasarımlar olmuştur, ancak bu malzemeler arasında birçok uygulama, biyouyumluluk ve optik özellikler gibi benzersiz avantajları nedeniyle ZnO nanomalzemelerini kullanmaktadır. Bununla birlikte, bu nanoteller, elektronik olarak ZnO içeren ve esnek bir harekete izin veren uyumlu bir ana malzeme gerektirir. Bu ihtiyaç ile ilgili olarak, ZnO nanoteller esnek gerinim sensörleri oluşturmak için sürekli olarak çeşitli malzemelere gömülüdürler. Bu tezde, GA'lar, ZnO piezoelektrik özelliklerinin her koşulda muhafaza edilebileceği mükemmel alıcı substrat özellikleri sağladığından, sentezlenen GA substratlarına gömülü ZnO nanotellerine dayanan esnek piezotronik gerinim sensörü üretmek için bir teknik geliştirilmiştir. Ayrıca, bu tanımlanmış gerinim sensörü, sentezlenen grafen aerojel substratı üzerinde kimyasal buhar birikimi yöntemi ile büyütülmüş ZnO nanotel filmi ile elde edilmiştir. Gerinim algılamanın, hem statik hem de dinamik yüklemenin, GA'ların, dikkate değer özelliklerinden ötürü ev sahibi materyal olarak umut verici adaylar olduklarını gösterdikleri bulunmuştur. Ek olarak, sensörün I-V karakteristiği, hem statik hem de dinamik yükler altında arzu edilen piezotronik özellikler, Schottky bariyer yüksekliğinde piezo potansiyel modüle edilmiş değişiklikler nedeniyle yüksek hassasiyet gösterir. Herhangi bir ZnO / Karbon bazlı gerinim sensörü

için gerinim faktöründen (GF) neredeyse % 50 daha yüksek olan 120' ye kadar yüksek bir GF göstermektedir.

Ayrıca, nanoteller, karbon nanotüpler ve iki boyutlu (2D) malzemeler de dahil olmak üzere nanomalzemelerin kullanılmasıyla giyilebilir cihazlar geliştirmek için çok çaba sarf edilmektedir. Özellikle grafen, mükemmel elektriksel ve mekanik özellikleri sayesinde giyilebilir uygulamalar için kapsamlı bir şekilde incelenmiştir. Bu konuda odak, iletken köpük ve nano kağıtlar gibi üç boyutlu grafen tabanlı sensör mimarileri üzerindedir. Bununla birlikte, tüm geometriler hala konformal entegrasyon ve hassasiyet ile ilgili bazı engellerle karşılaşmaktadır. Bu nedenle, bu tezde, istemsiz insan hareketinden bilgiyi etkili bir şekilde çıkaracak GA tabanlı gerinim sensörleri oluşturmanın yeni yöntemi gösterilmektedir. GA'lar, üç boyutlu hibrid çerçeveler üretmek için karbon nanotüplerle (CNT'ler) benzersiz bir şekilde güçlendirilmiştir. Bunlar, iletken yolların genellikle yüksek gerilme veya stres koşulları altında tutulduğu gerilebilir özellikler sağlamaktadırlar. İletken yolların korunması, güvenilir bilgi sağlamak için son derece önemlidir ve bu da gerinim sensörü tasarımları için zorlu problemlerden biridir. Bununla birlikte, GA ve CNTs karışımı, güvenilir veri toplama için mükemmel bir çerçeve sağlar ve malzeme işlevselleştirme özellikleri, hassas sensörler sağlamak için mükemmel bir fırsat sunmaktadır. Bu çalışma sırasında, CNT'lerle yeniden yapılanma ve basit, düşük maliyetli ve ölçeklenebilir olan dispersiyon tekniği ile oldukça işlevselleştirilmiş üretilmiş GA'dan bir gerinim sensörü hazırlanmıştır.

AKNOWLEDGEMENTS

I would first like to thank my dear advisor Asst. Prof. Onur Ergen for his precious guidance and support, as well as giving me the opportunity to pursue a master's degree in his interdisiplinary research group. It was an interesting experience for me that I have learnt so much more as compared to what I already knew. The door of Asst. Prof. Onur Ergen's office was always open whenever I ran into a trouble spot or had a question about my master's studies. He consistently guided this master's thesis to be my unique work, but steered me in the right the direction whenever he thought I needed it. His endless patience and optimism throughout all the problems encountered will always be appreciated. I truly acknowledge his help during the writing period of this master's thesis.
I would like to express my gratitude to Assoc. Prof. Uğur Ünal and Prof. Ali Çırpan for being my committee members and their valuable time.
I acknowledge the financial support of the Scientific and Technical Research Council of Turkey (TÜBİTAK) for the funding of project 118M068. I would also like to thank and acknowledge to Assoc. Prof. Dr. Uğur Ünal for his tolerance in using his laboratory for the synthesization part throughout the studies and I am gratefully beholden for his very worthful comments on this work.
I am truly grateful to Dr. Feriha Eylül Saraç Öztuna for her collaboration and guidance through the experimental procedures and methods in advance. Without her passionate participation and input, this master's studies could not have been successfully conducted.
I must express my very profound gratitude Dr. Hadi Jahangiri, Dr. Gülsu Şimşek Franci and Dr. Barış Yağcı not only for their continuous assistance with the facilities of Koç University Surface Science and Technology Center (KUYTAM) but also for their support and guidance in the SEM, XRD and RAMAN characterization parts of the studies. I am gratefully indebted to them and for their very valuable guidance.
As a member of Renewable Energy and Nano-electronics group (Re-ENGineering) and ENG 142 office, I had an opportunity to meet great people and make strong friendships. I would like to thank Gökçe İymen and Gizem Tanrıver for their endless friendship and supports. I would like to mention and thank Ahmet Hamdi Ünal and Mert Yusuf Erdolu that they have been precious colleagues for me since the beginning of my master's study in our projects. I am also very grateful to Buse Ünlütürk and Karim Sonbol for their support, valuable advices and having lunches mostly together.

I am also very thankful to Merve Yılmam, Pelda Akın and Kübra Nur Özvural for their endless support, friendship and spending great times together. I would also want to express my gratitude to my homemates in Koç University for their endless support and warm friendship.

My greatest thanks goes to my lovely friends Simen Bozkurt, Bartu Akın, Osman Akkuş, Ozan Yüksel, and Gülnur Soydam for being there for me whenever I need. I am also very thankful to my friends from METU: Bilge Nur Gezer, Perihan Aslı Özdal, Ekin Ersoy, Gamze Muratoğlu and Ferda Tekin for their endless support and friendship. I also thank my best friend Ege whose existence provided the driving force of this master's study. On every tiny second of this life, I am honored and thankful to be your best friend and everything.

Last but not the least, I am so grateful to my family for their presence but especially my most heartfelt appreciation goes to my lovely mother for providing me with unfailing support and continuous encouragement throughout not only this period of time but my whole life. I am so thankful for her always putting support behind me.

TABLE OF CONTENTS

LIST OF TABLES

LIST OF FIGURES

ABBREVIATIONS

AFM	Atomic force microscopy
BET	Branauer – Emmett – Teller
CA	Carbon aerogel
CNT	Carbon nanotube
CVD	Chemical vapor deposition
DI	Deionized water
FESEM	Field – Emission scanning electron microscopy
GA	Graphene aerogel
GF	Gauge factor
GO	Graphene oxide
HOPG	Highly oriented pyrolytic graphite
PDMS	Polydimethylsiloxane
PECVD	Plasma enhanced chemical vapor deposition
RFA	Resorcinol-formaldehyde aerogels
rGO	Reduced graphene oxide
SA	Silicon aerogel
SBH	Schottky barrier height
sCO_2	Supercritical carbon dioxide
STEM	Scanning transmission electron microscopy
XPS	X-ray photoelectron spectroscopy
XRD	X-ray Diffraction
ZnO-NW	Zinc oxide nanowire

Chapter 1:
INTRODUCTION

Carbon is so ubiquitous that it is located at the center of our lives and dominates existence in all aspects. Thus, it is one of the most intriguing elements in the periodic table. Carbon is essential for life, and its unique properties make it the basis of organic chemistry. Moreover, it has 5 allotropes, and the three well-known allotropes of carbon are diamond, carbon nanotube (CNT), and graphite [1]. Single-layer graphite is known as graphene and possesses fascinating properties which makes it a wonder material. Hexagonally arranged sp^2 hybridized carbon network creates graphene in which all carbons are bonded by σ-bonds in the lateral axis, and thus within the c-axis, interactions are very weak due to the lack of chemical bonding. Graphene provides excellent thermal, electrical, mechanical, and optical properties. For instance, it has a thermal conductivity of 4840-5300 W/mK, electron mobility that is larger than $2x10^5$ cm^2/Vs, the high surface area of 2630 m^2/g and high tensile strength around 130 GPa and modulus around 1000 GPa [2]. Due to these excellent properties that are mentioned, it is classified as a promising material that can replace silicon. Therefore, it has been attracted by studies in both academia and industry [3]. The number of studies has been increasing gradually since single-layer graphene was discovered by Novoselov and Geim in 2004 [4]. Several methods have been discovered to obtain graphene and these include both physical and chemical methods which are unrolling carbon nanotubes (CNT), mechanical exfoliation, ultrasonic cleavage, chemical vapor deposition (CVD), epitaxial growth on SiC, thermal reduction, chemical reduction, Hummer's method [5], [6]. Furthermore, the Hummer's method is considered as one of the most popular methods in terms of its convenience and industrial applicability at a low cost. It is possible to produce graphite oxide by the oxidation of graphite with extreme oxidizing agents in powder form and then, graphene oxide (GO) is formed by ultrasonic exfoliation of hydrophilic graphite oxide layers. Later, this obtained GO is reduced via various methods such as chemical, thermal, and electrochemical to produce graphene [7]. During this study, the concern is given to graphene aerogel synthesis using the path of modified Hummer's method in order to produce aerogels which are highly qualified that are scrutinized to be found as favorable for its applications.

Graphene aerogels (GAs) which demonstrate excellent features such as larger surface area and porous size with ultra-low density and thermal conductivity. Although they have been prepared to be used in various application areas from pollution adsorption to energy storage, thermal insulation and supercapacitor, they are lack of high mechanical properties that drag them to have poor electrical conductivity which restricts their wide application areas. Hence, they are mostly combined with other materials and form hybrid materials to remove their lacks for those application areas required high electrical conductivity. Hereby, graphene aerogels are beneficial not only because of possessing excellent properties and also, having the ability of being biocompatible for an intense scientific research area due to having several application areas related to wearable technology, health monitoring, environmental pollution, energy and electronic fields [8].

In the second chapter of this thesis, there is a wide breadth of literature survey reviewed on graphene and its derivatives, hybrid materials, and aerogels in order to make these more understandable for the rest of the thesis. In addition, the information about different synthesis methodologies used for graphene, graphene oxide and aerogels are investigated deeply in this section. Moreover, recent studies on aerogels and their application areas are also included in the second chapter.

The third chapter of the thesis consists of the experimental part in which materials and methodologies used to synthesize precursors and GA are explained. Therefore, GA is synthesized using precursors of GO solutions that is synthesized by modified Hummer's method, which is cross-linked via organic sol-gel chemistry, followed by super critical drying (sCO_2) and then carbonization, which is achieved through pyrolysis at 1050 $^{\circ}$C under nitrogen, as previously reported by [9]–[11]. Additionally, construction of the hybrid materials which are ZnO nanowires (ZnO-NWs) embedded in GA and GA/CNT hybrid structures are explained via synthesis methodologies used for its further applications. Moreover, techniques and characterization methods used are introduced during and after the synthesis.

In the fourth chapter of thesis, results are demonstrated via characterization methods used after the synthesis. Subsequently, this includes Raman spectroscopy, X-ray powder diffraction (XRD), Field – Emission scanning electron microscopy (FESEM) for the characterization of GA and the electrical characterization for the hybrid structures. Additionally, this chapter includes results and discussion of the synthesis and for its applications. Furthermore, all findings obtained, and the corresponding results as graphs

and images of the analysis made are listed and discussed in detail in this section of the thesis.

Last chapter of the thesis concludes the data obtained from this study and results. Moreover, the innovation that could be implemented as a result of this thesis is examined, and the suggestions are proposed for further studies.

Chapter 2:
LITERATURE SURVEY

In this chapter, the fundamental knowledge on graphite and its derivatives, hybrid materials and aerogels are built. Furthermore, different synthesis methods of graphene, graphene oxide and aerogels, and recent studies on aerogels and application areas in literature are reviewed.

2.1 *Graphite and Its Derivatives*

2.1.1 Graphite

Graphite is known as one the allotropes of carbon atom that can be either formed naturally or produced synthetically. It owns a hexagonal internal packing structure and was discovered by the Swedish chemist whom Carl W. Scheele in 1778. Compared to diamond, which is another type of allotropes of carbon atom, it is opaque with a much softer structure. Moreover, graphite structure is layered that makes it different from fullerene which is another type of allotropes of carbon atom. While graphite is one of the softest materials and has dyestuff feature, it is generally used in pencil nibs. On the other hand, scientific research demonstrated that the layered structure of graphite allows further reactions by opening [12]. Since the layered structure of graphite could open, it enables to produce graphene and graphene oxide materials. The allotropes of carbon atom are seen in Figure 2.1.

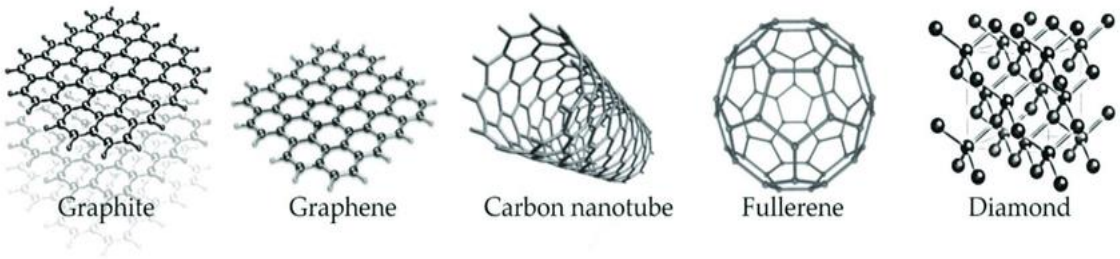

Figure 2.1: Allotropic forms of carbon atom: Graphite (3D), graphene (2D), carbon nanotube (CNT) (1D), fullerene (0D) and diamond (3D), respectively [13].

2.1.2 Graphene

Graphene is a single-layered and one-atom-sized nanoscale particle, which is the basic building block of all carbon allotropes in the structure, where regular carbon atoms are sp^2 hybridized in the hexagonal structure. Graphene, which has a unique molecular structure with its two-dimensional structure having a single atom thickness and strong bond structure between molecules, has very good electrical, electrochemical, thermal, optical, and mechanical properties [14]. Carbon atoms have the ability to make four bonds. As the two-dimensional graphene also makes three bonds, the fourth electron freely circulates in the crystal and thus, gives the graphene high conductivity. While electrons exposed in metals cause energy loss and heat generation, electrons at room temperature in graphene can cover quite long distances without any collision. Moreover, it is considered as 100 to 300 times stronger than steel. In addition to being flexible and transparent, it is the thinnest and lightest material known. Thanks to these properties and its application areas that are almost endless, it is one of the materials that are frequently researched today. For instance, different graphene-based materials that differs in functional properties and sizes are especially involved in polymer composites. Therefore, polar groups on the graphene surface improve compatibility with the polymer surface. The types of graphene obtained by the oxidation method are more suitable for surface formation as they bond due to functional groups in graphene-based composite production [15]. Graphene and its derivatives are shown in Figure 2.2.

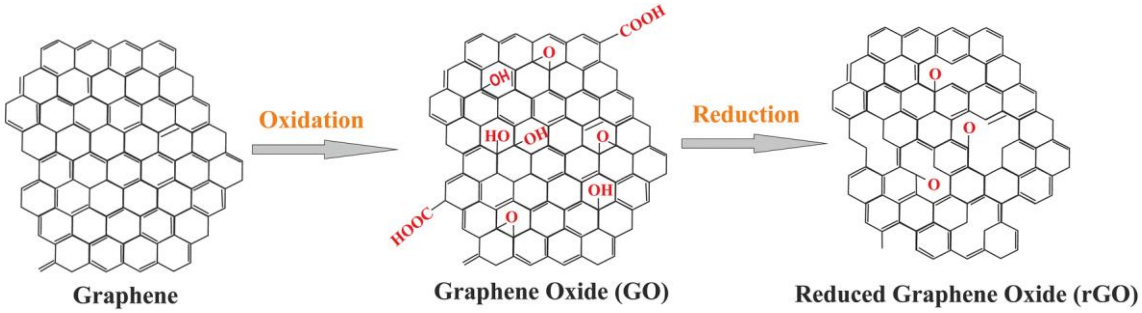

Figure 2.2: Graphene, graphene oxide and reduced graphene oxide structures [16].

2.1.3 Graphene Oxide (GO)

Graphene oxide is a two-dimensional (2D) material that contains oxygen and hydrogen atoms in its structure unlike graphene [15]. It is the oxidized form of graphene with

functional oxygen groups located on the sp^2 basal plane. It has been synthesized with Brodie, Staundenmaier, Offeman and Hummer's methods since the beginning of the 19th century. All the mentioned methods are based on the reaction of oxidation of graphite with strong acids and oxidants. The degree of oxidation varies depending on the method used, the reaction conditions, and the properties of graphite [17]. The physical properties of graphene oxide can be changed by removing its functional groups from its surface. This process converts the graphene oxide from semiconductor to the insulator. Due to its functional oxygen groups, graphene oxide is hydrophilic and soluble in water, whereas graphene is hydrophobic and insoluble in water [18]. Moreover, the best known and widely used graphene oxide synthesis method is the modified Hummer's method. With the help of this method, it becomes possible to obtain considerably high yield compared to other methods. In addition to this, this method is used frequently due to its cost is much lower than other methods. On the other hand, products used during synthesis are dangerous and poisonous, and toxic gases are released. The resulting graphene oxide slurry is very acidic and must be handled carefully throughout the whole production process. The structure of graphene oxide can be seen in Figure 2.3.

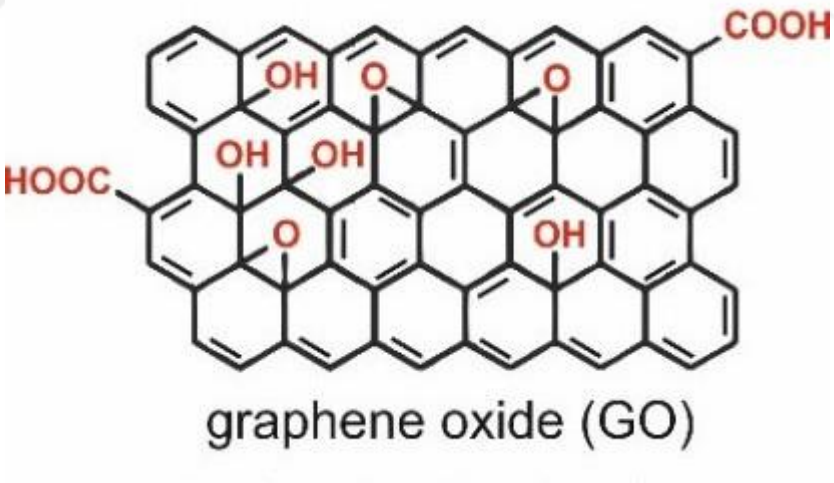

Figure 2.3: Graphene oxide (GO) structure [19].

2.1.4 Reduced Graphene Oxide (rGO)

There are several methods to obtain reduced graphene oxide (rGO) from graphene oxide solutions. Among these methods, thermal oxygenation reduction, photoreduction, electrochemical reduction, and chemical reduction are the most common methods [20]. Thermal deoxygenation method requires to carry out under vacuum, inert atmosphere, or

a reduced gas such as H_2 [21]. Functional groups of graphene oxide decompose to CO or CO_2 and the reduction temperature and duration time indicate the reduction degree of C/O ratio with the electrical conductivity of rGO that is produced [22]. Although this method is energy consuming, still it is considered as an effective process to produce rGO. Photoreduction method applies irradiation with UV light source to the GO sheets under an ambient or inert atmosphere [23]. Thus, a photoreaction occurs as a result that leads to a production of CO_2 and H_2 molecules. By using voltammetric or chronoamperometric techniques, it becomes possible to produce rGO and this method is known as electrochemical reduction which is a clean alternative method [24]. Finally, chemical reduction method is more beneficial due to its effectiveness and less energy consumption. In addition to this, final products are more diverse chemically because of the type of the reducing agent used during reduction. Hydrazine is the most used reducing agent, among others. Therefore, it can produce high C/O ratio rGOs with an electrical conductivity under mild conditions [25].

2.2 Synthesis Methods of Graphene and Its Derivatives

2.2.1 Graphene Synthesis Techniques

Different synthesis methods of the graphene enable to obtain the specific product on the desired size, purity, and efflorescence. Graphitic thin films have been obtained by various techniques since the earlier ages. Later, few-layer graphite on a single crystal platinum surface was synthesized by CVD method in 1975. However, graphene was not designated due to the unadvanced characterization techniques or the lack of their applications [26]. Back then, the investigation on their electronic properties never were carried out since it was difficult to isolate and transfer them on the surface of insulating substrates. Although, Ruoff and his colleagues worked on the isolation of thin graphitic creatures that are flakes placed on SiO_2 substrates with the help of highly oriented pyrolytic graphite (HOPG), their electrical properties were not characterized and reported [27]. Yet, in 2005, Kim and his colleagues were achieved to report their electrical properties with the help of similar method used by Ruoff et al. [28]. This report played an important role for the advancement of graphene research, and thus Geim and his coworkers were the first to succeed on publishing their work. Subsequently, graphene was discovered in 2004 and this discovery leaded to development of various techniques to produce few layers

graphene. Moreover, 2D crystals were obtained in 2004 and the first exfoliation from the bulk counterparts of thin flakes of graphene and other materials such as molybdenum disulphide, niobium diselenide, and hexagonal boron nitride was achieved in 2005. On the other hand, graphene was in the form of small flakes when it was first obtained via mechanical exfoliation of graphite that used scotch tape [29], [30]. This method was able to give the highest quality product of graphene for the mass production, however there was a need for the fabrication method which can synthesize graphene in wafer scale. Regarding this need, various techniques for graphene synthesis have been developed. Among these various techniques, chemical exfoliation, mechanical exfoliation, chemical synthesis, and thermal chemical vapor deposition (CVD) have become the most used methods for the synthesis of graphene today [2], [31], [32]. Additionally, unzipping nanotube and synthesis via microwave methods are also reported. Atomic force microscopy (AFM) cantilever used in mechanical exfoliation and this enables to fabricate few layers graphene, however the thickness of graphene is limited that varies to 10 nm compared to 30-layer graphene. Chemical synthesis process consists the synthesis of graphite oxide that is dispersed in a solution and the reduction reaction with hydrazine. In chemical exfoliation method, large alkali ions are inserted between the graphite layers and this enables the exfoliation of solution dispersed graphite. Catalytic thermal chemical vapor deposition (CVD) method has verified as the most outstanding technique for the carbon nanotube synthesis in large scale graphene production. CVD process is considered as thermal CVD when it is carried out in a resistive heating furnace, whereas it is called as plasma enhanced CVD (PECVD) if the process consists plasma assisted growth. Eventually, all the synthesis methods demonstrate some drawbacks which depend on the desired final application of graphene. For instance, the mechanical exfoliation method fails to obtain similar structures, but it has the capability to fabricate monolayer to few layers of graphene which varies in sizes. Moreover, chemical synthesis methods are carried out at low temperatures that facilitates the multi types of substrates fabrication of graphene at ambient temperatures. Although the produced graphene, by this method, have larger area sizes, they are non-uniformed and dispersed. Also, graphene which was synthesized from reduced graphene oxides (rGOs) effects graphite oxide reduction to become incomplete which leads to a successive debasement of its electrical properties that depends on degree of reduction. Nevertheless, thermal CVD methods are more beneficial to fabricate larger area devices and convenient to use for the replacement of Si

[33]. Epitaxial graphene synthesis is another method that helps to graphitize the surface of SiC. Since it is carried out at high temperatures, it is incapable of transferring on another substrates. Thus, the thermal CVD method is second to none due to its ability to produce uniform layer carbon atoms which are thermally and chemically catalyzed. It can also be deposited on the surfaces of metals with the ability of being transferred on a wide range of other substrates [34]. Figure 2.4 shows an overview of the techniques on graphene synthesis as a flow chart.

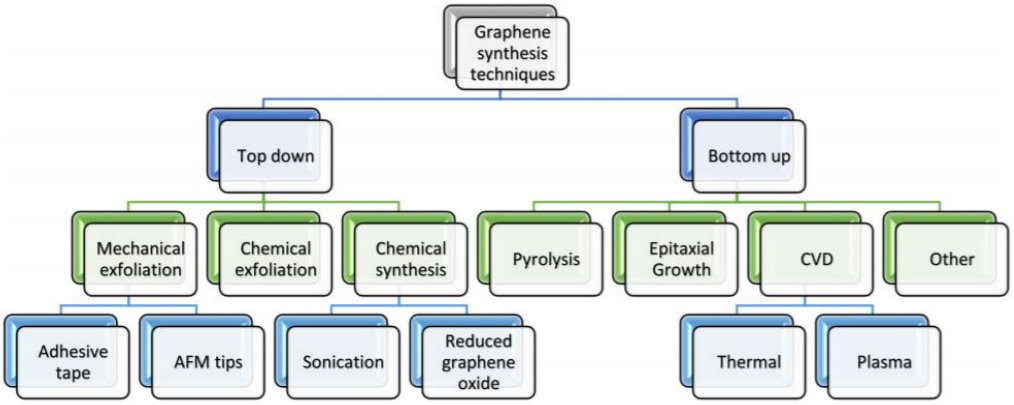

Figure 2.4: An overview of graphene synthesis techniques [35].

2.2.2 Graphene Oxide (GO) Synthesis Techniques

Graphene oxide synthesis constitutes the first step of the chemical synthesis methods carried out to obtain graphene in the solution phase. For this purpose, graphite oxide is obtained by connecting various functional groups that are oxygenated to the basal plane of each of the two-dimensional planar carbon layers in the structure of the graphite and to the corners of the its layers. The graphite oxide structure is also called graphitic acid, and the monolayer of this stacked structure is defined as graphene oxide (GO) [36]. The structure of GO was first introduced by the English chemist B. C. Brodie in 1859. He managed to obtain graphite oxides by examining the reactivity of graphite flakes with potassium chlorate and fuming nitric acid [37], [38]. After it was discovered in 2004, graphene has become more attractive to researchers and the oxidized from of graphite began to be called as GO. Although there is no clear difference in between the chemical structures of graphene oxide and graphite oxide, there is a general terminology used in literature that the state of the material in solution or suspension is expressed as graphene

oxide (GO) and the state in the solid or film phase as graphite oxide [39]. In addition to this, graphene oxide is not existed naturally, but it was obtained by synthesizing a century ago. In literature, four main methods, which are Brodie, L. Staudenmaier, Hummer's, and Tour methods, are carried out to obtain graphene oxide synthetically. Additionally, novel synthetic methods with several modifications to those fundamental methods have been proposed in recent years. Four main methods with their oxidizing agents and reaction mediums are shown in Table 2.1.

Table 2.1: Methods to produce graphene oxide (GO).

Method	**Oxidizing Agent**	**Reaction Medium**
Brodie	$KClO_3$	HNO_3 and H_2SO_4
L. Staudenmaier	$KClO_3$	Fuming HNO_3
Hummer's	$KMnO_4$ $NaNO_3$	Concentrated H_2SO_4
Tour	$KMnO_4$	H_2SO_4 and H_3PO_4

Graphene oxide (GO) was first synthesized by Brodie in 1859. He obtained a novel compound which contains carbon, oxygen, and hydrogen by preparing graphite in $KClO_3$ and fuming HNO_3. Obtained products were dried at 100 °C and oxidation was repeated three times. According to his results, light yellow colored product was obtained by repeating all the steps to enhance to oxidization and GO was observed as soluble in basic medium whereas not soluble in acidic environment. Therefore, obtained product was called as graphitic acid by his study [37]. After the study of Brodie, L. Staudenmaier aimed to improve his method. Thus, potassium and sodium chlorate aliquots added in multiple steps and concentrated H_2SO_4 was used in order to increase the acidity of the environment. As a result, this method could proceed as a single reaction and more GO was obtained compared to Brodie's method [40]. After 60 years from L.Staudenmaier's study in 1958, a mixture of concentrated H_2SO_4 and $NaNO_3$ with $KMnO_4$ as a catalyst was used in Hummer's method. Hummers and Offeman reported that oxidation process took only 2 hours and it was carried out under 45 °C. Furthermore, dilution and hydrogen peroxide treatment steps were proceeded to obtain as a yellow-brown colored residue of higher oxidation degree product. This method is considered as eco-friendly since ClO_2

gases are not generated at the end [7]. Additionally, several different modified Hummer's methods, which differs in reaction conditions, oxidant types, and quantities changed, have been developed in literature. In 2010, Tour method was proposed by Tour and his group in Rice University. The amount of $KMnO_4$ was increased and a mixture of H_2SO_4 /H_3PO_4 with a ratio of 9:1 was used. Since the usage of $NaNO_3$ has been removed from the reaction medium, this method has become advantageous. Hence, deleterious gases, such as NO_2, N_2O_4 or ClO_2, are not generated during the reaction due to the lack of $NaNO_3$. Also, GO products are obtained with a higher oxidation degree compared to Hummer's method [18]. Seeing that, several methods with some drawbacks and benefits have been developed to enhance the oxidation degree of graphene oxide production. Therefore, ClO_2 gas, which is harmful, is produced as a side product in the methods of Brodie and L. Staudenmaier. On the other hand, generation of ClO_2 gas was eliminated by Hummer's method and it has become the most used method, among others. Tour method achieved to prevent the formation of toxic NO_x gases by using phosphoric acid instead of $NaNO_3$ and avoids the further oxidation of the basal plane that provides pinhole free sp^2 plane. Besides, graphite source plays a crucial role to produce GO since the properties of the starting materials affects the properties of the end product in terms of crystallinity, defect density, reactivity and dispersibility.

Thus far, different methods to synthesize graphite oxide was introduced, but exfoliation step, which does not occur spontaneously, is required to obtain monolayer GO. Therefore, either thermal or mechanical exfoliation can be used for this purpose. Sonication, stirring or both are considered as mechanical exfoliation methods used. Graphite oxide can be converted into GO in water or polar organic solvents completely via these methods. Moreover, sonication causes not only the decrease in sheet sizes from microns to nanometers but also broadening the distribution of sizes of GO sheets [41]. GO dispersibility in water varies in between 1-4 mg/mL [42]. Additionally, it is also dispersible in organic solvents such as dimethylformamide (DMF), N –methyl pyrrolidone (NMP), and tetrahydrofuran (THF) [43]. On the other hand, thermal exfoliation is carried out at minimum of 550 °C to proceed the exfoliation successfully. The formation of H_2O, CO_2, and CO gases occurs during heating due to the decomposition of oxygen-bearing functional groups on the basal plane of graphite oxide. If the decomposition rate of these functional groups gets higher than the diffusion rate of these gases through the lateral direction, then van der Walls interactions between the

layers are prevailed over by the increase in interlayer pressure. As van der Walls interactions are broken, the distance gets increased in between the layer and as a result, exfoliation occurs [44].

2.2.3 Reduced Graphene Oxide (rGO) Synthesis Techniques

Reduced graphene oxide (rGO) and its derivatives have become promising materials because of their usability in many fields such as energy storage, detector research, and purification studies [4], [45]. The second step in the synthesis of graphene with the chemical method is the reduction of GO by various processes such as chemical, thermal, photothermal, laser-induced, and electrochemical. After the reduction process, the oxygenated functional groups in the layers are largely removed and the conjugated structures in which the π electrons can be delocalized are reconstructed in the system. Thus, reduced GO (rGO) layers with electrical conductivity are formed [46]. The reduction efficiency is determined by carbon to oxygen ratio. Depending on the type of reduction, reducing agent, reduction time and temperature, reaction parameters such as annealing time and temperature, the ratio changes between 4:1 and 80:1. Moreover, the conductivity values of the layers vary in a wide range as well. Reducing agents used in chemical processes are mostly toxic and hazardous such as hydrazine monohydrate, dimethyl hydrazine, sodium borohydride, hydroquinone, hydroxyl amine, p-phenylenediamine and sodium hydrosulfite [47]–[49]. Therefore, it is necessary to limit the use of these reducing agents and provide less harmful synthesis conditions for production of rGO in high amounts. Although Fe, Al or Zn metal powders, hydrogen halides, Vitamin C (L-ascorbic acid), D-glucose, various alcohols, acetic acid, dextran and tea solutions in the acidic medium allow rGO synthesis to be performed under more mild conditions, the low degree of reduction becomes an obstacle to overcome with. To overcome with this problem, the reduction reaction temperature is set to higher than 25 °C and duration time is increased. In addition to this, studies on dispersion stability are carried out to prevent rGOs from settling and agglomerating due to the removal of functional groups from the layers in the solvent medium. Graphene derivatives with dispersion stability can be used in molecular electronic application fields, which include direct wet coating methods and film preparation techniques. This clearly emphasizes the importance of the stability of graphene dispersions for the widespread use of chemically

synthesized graphene. In addition to chemical reduction method, GO solutions can be thermally reduced under vacuum at high temperatures such as 1000-1100 °C. Although this method is easy and environmentally friendly, it is not preferred for the high capacity rGO synthesis because it causes a lot of energy consumption [50]. Moreover, electrochemical, microwave, and photocatalytic reduction methods are also among the non-preferred methods due to their low efficiency [48], [51], [52]. Overall, GO reduction is done in order to obtain graphene-based material which is dispersible. Graphene oxide reduction yields graphene in gram scale likewise its production is a low-cost process. Among all reduction methods mentioned, ultraviolet assisted reduction method is preferable due to being a green treatment process without the generation of any toxic pollutant or reductants. Additionally, direct reduction of GO can be carried out only under UV lamp [53]. Also, conductivity (S/m) values and C:O ratios of rGOs obtained by various studies via different methods are demonstrated in Table 2.2.

Table 2.2: Conductivity (S/m) values and C:O ratios of rGOs obtained by various studies via different methods.

Studied by	**Type**	**Reduction Condition**	**Reduction Method**	**C:O Ratio**	**Conductivity (S/m)**
(Mohan et al.,2015) [54]	rGO	72h with HI HBr Hydrazine	Chemical	14.92 9.92 6.75	10330 5500 3300
(Chen et al, 2016) [55]	rGO	2466.85 °C	Thermal	81.64	311200
(Park et al., 2014) [56]	rGO	24h with N,N-dimethylhydrazine at 80 °C	Chemical	-	1900
(Zeng et al., 2014) [57]	rGO	Hydrazine-cetyltrimethyl ammonium chloride (CTAC)	Chemical	-	22300

(Stankovic et al., 2006) [58]	PS-rGO Composite	Dimethyl hydrazine	Chemical	-	1
(Ren et al., 2011) [59]	rGO	Hydrazine monohydrate	Chemical	15.51	500
(Zhou X. et al., 2011) [60]	rGO	Hydroxylamine L-ascorbic acid Hydrazine	Chemical	9.7 5.7 10.3	1122 800 1187
(Chen et al., 2009) [61]	rGO	p-phenylenediamine	Chemical	7.4	15000
(Zhou T. et al., 2011) [62]	rGO	Sodium hydrosulfide	Chemical	-	1377
(Pham et al., 2011) [63]	rGO	N-methyl-2-pyrrolidone	Chemical	9.68	21600
(Fan et al., 2011) [64]	rGO	30min with Fe/HCl at 25 °C	Chemical	7.9	2300
(Fan et al., 2010) [65]	rGO	30min with Al/HCl at 25 °C	Chemical	18.60	2100
(Dey et al., 2012) [66]	rGO	2h with Zn/HCl at 25 °C	Chemical	21.22	3416
(Mei and Ouyang, 2011) [67]	rGO	1min with Zn/HCl at 25 °C	Chemical	33.5	15000
(Pei et al., 2010) [68]	rGO	55% HI at 100 °C	Chemical	16	29800
(Moon et al., 2010) [69]	rGO	HI-acetic acid at 40 °C	Chemical	6.66	30400

(Zhang J. et al., 2010) [70]	rGO	48h with L-ascorbic acid at 23 °C	Chemical	-	800
(Fernández-Merino et al., 2010) [71]	rGO	15 min with 2 mM Vitamin C at 95 °C	Chemical	-	7700
(Chen, D. et al., 2011) [72]	rGO	72h with L-cysteine (amino acid) at 26 °C	Chemical	-	0.124
(Kim et al., 2011) [73]	rGO	3h with Dextran at 95 °C	Chemical	-	1.1
(Lei et al., 2011) [74]	rGO	10h with Tannic acid at 80°C	Chemical	2.44	656.7
(Mattevi et al., 2009) [45]	rGO	1100 °C	Thermal	12.5	~55000
(Vallés et al., 2012) [75]	rGO	30 min, under Ar atmosphere at 700 °C 30 min, under H_2 atmosphere	Thermal	1.2 28.57	8100 5000
(Park et al., 2012) [76]	Phenyl-Graphene (R-Ph-GO)	6h with 4-iodoaniline aryldiazonium salt at 300 °C	Thermo-Chemical	7.1	42000
(Guo et al., 2009) [77]	rGO	10 mmol/L PBS (K_2HPO_4/KH_2PO_4) at -1.5 V and pH 5	Electro-Chemical	-	3500

2.3 *Hybrid Materials*

The latest technological developments and the desire for new applications create great demand for novel materials. Many of the well-known materials such as metals, ceramics or plastics cannot fulfill all technological requirements for various new applications. Scientists have already noticed that mixtures of materials can show superior properties compared to their pure counterparts. One of the most successful examples is the composite group formed by incorporating a basic structural material into a second substance or matrix. Structural building blocks in these materials included in the matrix are predominantly inorganic and show a size range from micrometer to millimeter, and therefore their heterogeneous composition is mostly visible [78]. Later, it became obvious that reducing the dimensions of the inorganic units to the same level as the organic building blocks could lead to more homogeneous materials which allow the properties of the materials to be better adjusted at the molecular and nanoscale level. Even though the first appearance of hybrid materials is not completely obvious, it is reported as the mixing of organic and inorganic components was carried out in the ancient world. In ancient times, the production of bright and colored paints was the driving force to continuously try new paints or inorganic pigment mixtures and other inorganic and organic ingredients to create paints used thousands of years ago. For this reason, hybrid materials and even nanotechnology are not an invention of the last decade, but they were developed a long time ago. However, due to the availability of new physicochemical characterization methods performed by scientists in the 20^{th} and early 21^{st} centuries, the nanoscience field opened many perspectives for approaches to new materials. The combination of different analytical techniques brings new perspectives to hybrid materials and clearly reveals that bottom-up strategies for the design of molecular-level materials will lead to new features in this class of materials [79]. In addition to using inorganic materials and organic polymers like rubber as fillers, it has been a long time since inorganic and organic materials were being mixed. However, Sol-gel method which is a method of production of mixtures has changed this situation. This method, which will be discussed in detail later, was developed in the 1930s by using silicone alkoxides as the leading materials from which silica was produced. In particular, the silicone-based sol-gel process was one of the main driving forces, which has become a wide area by the production of inorganic-organic hybrid materials. The reason for using silicone is its processability and stability

of the Si-C bond during the formation of a silica networks which allow the production of organically modified inorganic networks in one step [78], [79]. Inorganic and organic hybrid materials are applicable in many different areas of materials due to their easy processing method and them being suitable for a design on a molecular scale. Currently, there are four main issues in the synthesis of inorganic - organic materials that are molecular engineering, nanometer and micrometer size organization, transition from single functional to multifunctional hybrids and their combination with bioactive components [79]. Hybrid material is a term used for many different systems covering a wide range of different materials, such as crystalline high order coordination polymers, amorphous sol-gel compounds, and materials which interact and do not interact with inorganic and organic units. From a broader perspective, hybrid material can be defined as a material that contains a mixture of two materials on a molecular scale. Commonly, one of these compounds is inorganic and the other one is organic [78]. Furthermore, they are distinguished based on their possible interactions linking inorganic and organic species. Class I hybrid materials are those that show weak interactions between the two phases, such as van der Waals, hydrogen bonding, or weak electrostatic interactions. On the other hand, class II hybrid materials are the ones which demonstrate strong chemical interactions between components. Eventually, there is a continuous transition between weak and strong interactions due to the gradual change of the strength of chemical interactions. In addition to their bonding properties, their structural properties can also be used to distinguish between various hybrid materials. The organic part containing the functional group that allows binding to an inorganic network can act as a modifying compound in the network because of the inorganic network in the structure of the final product is replaced only by the organic group [78]. For instance, trialkoxysilane and phenyltrialkoxysilanes are examples for these compounds. In the sol-gel process, they modify the silica network by reacting the trialkoxysilane group without providing any additional functional groups intended to further react to the formed material. If a reactive functional group is added to the system, this group is called a network functionalizers. Moreover, if two or three anchor groups replace an organic segment, then this becomes hybrid network which is an integral part of the inorganic group.

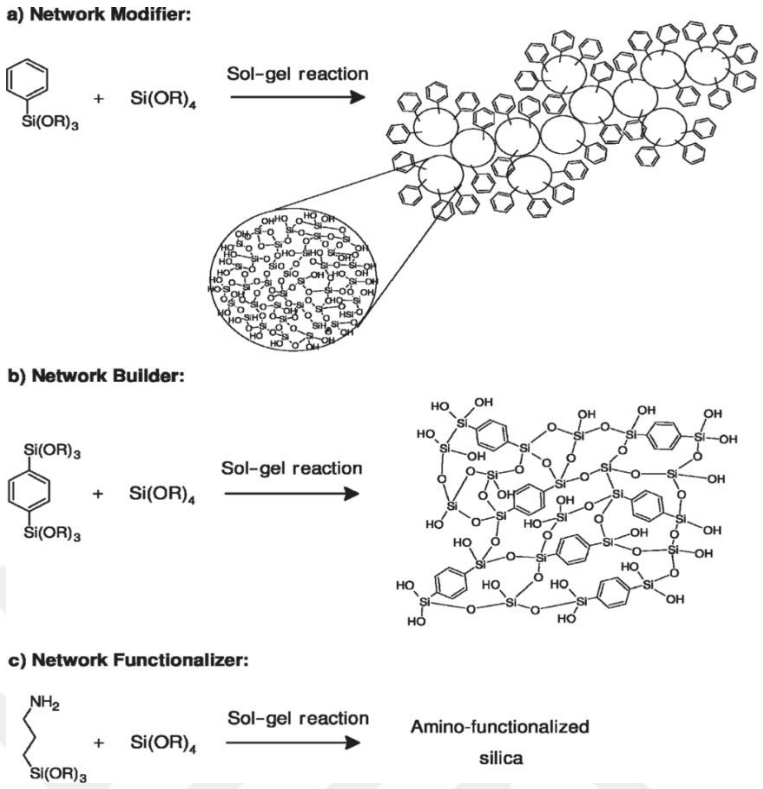

Figure 2.5: Organically functionalized trialkoxysilanes, R′Si(OR)$_3$, used as a) modifier; b) builder and c) functionalizer of silica-based network through the sol-gel process [80].

If there is not any strong chemical interaction between inorganic and organic building blocks, then mixtures are formed. For instance, the combination of inorganic clusters or organic polymers that do not have strong interactions such as covalent bonds between particles can be given as an example. Due to the functions of the components, a material with a compressed discrete inorganic part is obtained, which is stuck in the polymer crosslink due to weak cross-linking by inorganic units intertwined by physical interactions, or because inorganic components are trapped. If an inorganic and organic network encompasses each other without any strong chemical interactions with each other, interpenetrating networks are formed. For example, a sol-gel material is formed in the presence of an organic polymer. Both materials described belong to class I hybrids. On the other hand, class II hybrids are formed when discrete inorganic building blocks, for example, clusters, are covalently bonded to organic polymers, or when inorganic and organic polymers are covalently bonded with each other [78].

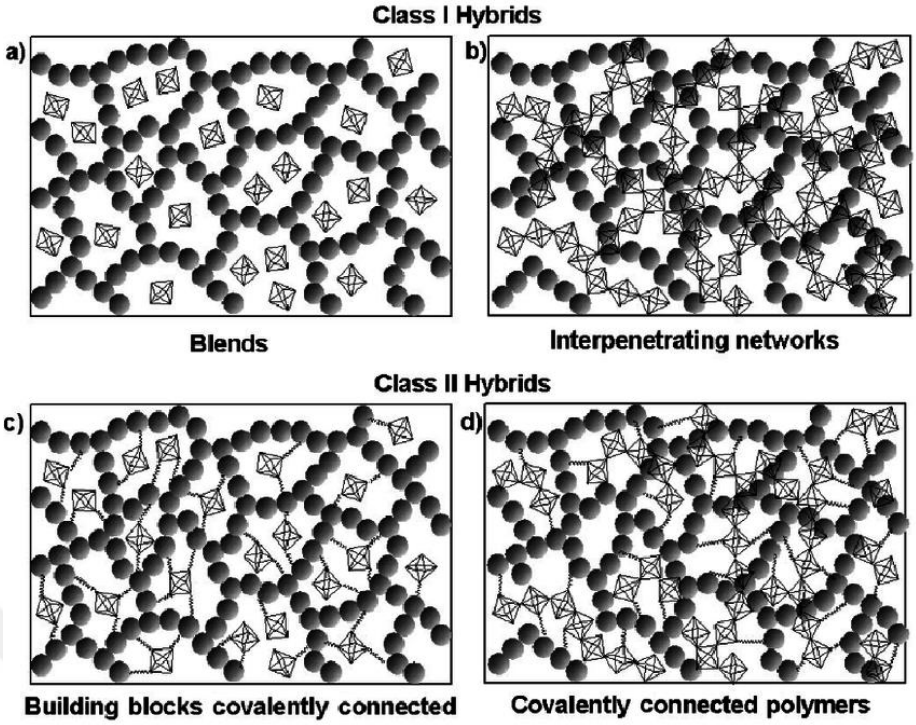

Figure 2.6: The structures of class I and class II hybrid materials [78].

2.4 *Aerogels*

Aerogels have been attracted to researchers in recent years due to their unique properties. These fascinating features are the result of the distributions of solid networks. Their extremely high porous structure and high surface area give them these unique properties and make them promising candidates for various applications. These low-density materials are transparent, have very low thermal conductivity, but are very fragile and absorb moisture causing degradation [79]. Some of the common properties of aerogels are shown in Table 2.3.

Table 2.3: Common properties of aerogels.

Properties	**Values**	**Conclusion**
Density	~0.003 g/cm^3	The lowest density solid material [81].
Porosity	80 – 99.8 %	High porosity [81], [82].
Surface Area	500 – 1200 m^2/g	Concluded by BET analysis [81], [82].

Average diameter of pores	20 – 150 nm	Mostly in the mesoporous range [81].
Thermal conductivity	0.017 – 0.021 W/m.K	Very high thermal insulation [82].
Thermal resistance	500 ºC	Shrinkage starts at 500 ºC and altered by the increase in temperature. Melting point is at 1200 ºC [83].
Dielectric constant	1.0 – 2.0	Low value compared to solid materials [81].
Young's Modulus	0.002 – 100 MPa	Very low value compared to solid silica [82].
Poisson's ratio	0.2	Similar to dense silica [82].
Refractive index	~1.05	Low value compared to solid materials [81].
Optical properties	>90%	According to permeability measurement done at 630 nm [83].
Speed of sound	100 m/s	One of the lowest speed materials in solid materials [81].

As stated before, aerogels are low density microporous solids with a fine, open-pore structure that leads to high porous and wide surface areas. These features make them unique in many applications and allow to be used for many applications, some of which have already been commercialized. There have been many debates going on the definition of aerogels in recent years. According to Smirnova and Gurikov, an aerogel has been defined as an open colloidal or polymeric network of loosely packed, bonded particles or fibers, which are expanding throughout their volume by a gas and, thus exhibiting a very low density and high specific surface area [84]. Although the production method of

aerogels is not included in this definition, they are generally formed by a starting gel without significant volume reduction, network compression or network degradation. The starting gel can consist of almost any material or different combinations which are called as hybrid aerogels. Aerogel and its derivative materials are known as the lightest solid material in the literature. The density of conventional silica type aerogel is around 0.001 g/cm^3. The reason why it has such a low density is that 99.98% of its volume is composed of air. The most important reason for the limited application of classical aerogels is that they are fragile due to the silica groups in their structure and cannot bear any load. Thanks to the cross-linking mechanism, the fragile aerogel gains a flexible structure and becomes capable of carrying loads. The term aerogel was first introduced by Steven Kistler in 1932 as gels in which the liquid was replaced with a gas without disturbing the gel-solid network structure [85]. In their first work, Kistler synthesized a series of aerogels that vary in their internal structures. Moreover, organic cellulose aerogels, nitrocellulose, gelatin, agar, or egg gels containing albumin, tungstic, ferric, tin oxide and nickel tartrate containing metal matrix aerogels were synthesized. In addition to silica aerogels, which can be processed relatively easily compared to other gels, he also managed to make alumina aerogels, which proved to be very weak mechanically. While wet gels were previously dried by evaporation, Kistler applied a new supercritical drying technique in which the liquid from that it absorbed the gels was evacuated after being converted into a supercritical fluid [85]. Basically, supercritical drying relies on heating a gel in an autoclave until it exceeds critical temperature (Tc) and critical pressure (Pc) of the liquid held in the gel pores. Kistler have also applied the super critical method to other liquids which are ethyl ether and liquid carbon dioxide used in an unsuccessful attempt to make propane and rubber aerogels. Taking into account the recent advances in the synthesis of aerogels, it would be more realistic to describe these materials as gels where the liquid is displaced by air, by shrinking the solid network, referring to the initial idea of Kistler. Furthermore, this definition illustrates the main difference between aerogels and xerogels. The term xerogel is defined by IUPAC as an open network created by removing all blowing agents from the gel. In the literature, studies on classical and cross-linked silica aerogels are frequently seen. Tajiri et al. examined how supercritical drying affects the structure and properties of the silica aerogel [86]. In their study, supercritical drying was carried out by using methanol, ethanol, and 2-propanol. As a result of the study, the most shrinkage was observed in the synthesis route with 2-propanol. Ethanol and methanol

showed the lowest shrinkage. In bending strength, a certain change was not observed in the drying process with different materials. Additionally, there are other important studies done by Leventis and his friends in this field [87]. Unlike others, they investigated the method of aerogel synthesis without the supercritical drying process. As a result of washing 4 times with pentane under room conditions, it was observed similar results to the aerogel made with supercritical drying was obtained. The initiator chemicals commonly used in the literature were TMOS and TEOS. Capadona et al. prepared three systems with four different silane concentrations, four different di-isocyanate concentrations and two different temperature conditions, and as a result they synthesized 28 different monolithic aerogels [88]. As a result of their study, it has been observed that the highest density crosslinked aerogel has the highest tensile strength and elastic modulus. In addition to this result, the prepared cross-linked aerogels have a density up to 3 times higher than conventional silica aerogels but have 120 times more tensile strength. Katti et al. modified the classic aerogel with amine to determine their load bearing capacity with three-point bending test and dynamic mechanical analysis [89]. Specific compressive load yield strength of samples is 8900 Nm/kg with an average density of 0.478 g/cm^3, maximum compressive tensile strength is 186 MPa, yield point value is 3.89x10^5 Nm/kg, while young module of classical silica aerogel is around 92 MPa and determined around 130 MPa of crosslinked aerogel [89]. As aerogels are synthetic widely used materials in literature, they are classified by the composing material. Furthermore, the commonly studied known aerogels are silica, organic resorcinol formaldehyde (RF), carbon nanotube (CNT), carbon, and graphene aerogels.

2.4.1 Common Types of Aerogels and Their Synthesis via Sol-Gel Method

Silica Aerogels (SAs)

During the synthesis of silica aerogels (SAs), sol-gel process starts the first. Then, tetraethylorthosilicate (TEOS) or tetramethylorthosilicate (TMOS) are mixed with water in a solvent as ethanol or methanol. As a result, colloidal particles are independently formed, and they are existed in solution as dispersed. Moreover, they have crosslinked structures and this colloidal part of the suspension is known as sol. The other parts have the interconnected rigid network which consists pores that are filled by liquid and this part is called as the gel composed of 3D silicon oxide [90], [91]. Thanks to the intriguing

properties of obtained monolithic or granular SAs, they can be used in many applications. They possess low thermal conductivity as in between 0.017-0.021 W/mK, very low density in between 3-400 kg/m^3, transparency and high surface area as 500-1200 m^2/g. Thus, they can be used in Cherenkov detector because of their appropriate optical properties which are transparency and low refractive index [25], [92]. As SAs have very low thermal conductivity, they can be used in insulating materials in buildings or space vehicles [93], [94]. They can also be applied to gas phase reactions, adsorbents, and sensors as catalyst support due to having low density and high surface area [95], [96]. Moreover, they are promising materials as transparent conductors since they can be loaded with conductive materials.

Organic Aerogels (RFAs)

First, Pekala developed organic resorcinol-formaldehyde aerogels (RFAs) by using organic monomers which are resorcinol (R) and formaldehyde (F) via polycondensation reaction in 1989 [97]. In addition to this, phenol-furfural and melamine-formaldehyde can be used as reactants to produce organic aerogels [98]. These produced organic aerogels have high surface areas with high mesoporosity. Their density varies from 100 to 500 kg/m^3 and, they have a surface which can be functionalized. Subsequently, they are used as a precursor of carbon-based aerogels and promising candidates for adsorbents, catalyst that support gas phase reaction and sensors.

Carbon Aerogels (CAs)

RFAs are used as a precursor to prepare carbon aerogels (CAs) via carbonization that is carried out by the heat treatment of the sample in 500-2500 °C under N_2 or Ar atmosphere [99]. During carbonization, highly pure carbon structure is given to make an enrichment of carbon content in aerogel and functionalities of hydrogen and oxygen are lost by the organic aerogel. CAs gets electrically conductive after carbonization occurs about 750 °C. Then, it is also considered as stable in both acidic and basic conditions [100]. Moreover, they are distinguishable from other carbon-based materials that they are mesoporous which can be synthesized as monolithic materials and also, they possess high surface area as 400-1200 m^2/g, low density and high porosity [101]. Compared to other activated carbons, they show higher electrical conductivities. Since CAs have microstructural and physical properties that can be adapted into nanometer scale with

changing the parameters of steps used in sol-gel process, they have been attracted to studies on engineering products and applications in electrochemical super capacitors, catalyst support, insulators, broadband non-reflective materials and adsorbents [102], [103].

Graphene Aerogels (GAs)

Graphene aerogels (GAs) are type of aerogels which are made of graphene sheets that are randomly stacked. They demonstrate similar properties of graphene and bring together the features of aerogels. Since Xu. et al. reported the method of hydrothermal synthesis for the production of GAs in 2010, it has become one of the most commonly used technique to produce GAs in literature [104]. During the hydrothermal synthesis, graphene oxide (GO) solutions are dispersed in solvent such as water in a closed vessel and heated until a monolithic aerogel structure is occurred. GO solutions are the precursor to produce GAs due to having functional groups that can be reacted to other compounds and thus, yield new materials. Therefore, GO sheets are reduced simultaneously because of heat and pressure applied during the synthesis. Hu et al. studied on the production of GAs with thermogravimetric analysis that he reported as CO_2 entrapping occurs between GO layers which are reduced. Then, this results porous network formation [105], [106]. Furthermore, GAs are in more compact structural form and demonstrate high mechanical strength when acidic GO solutions are used. Cheng et al. [107] reported that GAs show high mechanical strength, specific and high surface area, high porosity, thermal and electrical conductivity, high specific capacitance, and high cyclic stability. Additionally, GAs are lighter than even air, and this explains the reason for graphene can be a substitute of helium which is rare and expensive relatively than graphene. All these fascinating features make GAs anticipated to be used for energy storage, supercapacitors, waste removal and gas sensing applications. Moreover, they are also suitable for the air purification as well as being a candidate as solar light photocatalysts. Since GAs allow the addition of nanoparticles, this enhances their properties and give a birth to new application areas [8].

Synthesis of Aerogels

In this heading, the hydrolysis and condensation reactions that lead to a solid-state network via synthesis method of sol-gel and drying process will be briefly described for

a better understanding of the synthesis of aerogels. Thus, synthesis of aerogels consists of two main parts which are sol-gel synthesis process and drying process. The basic scheme of the synthesis of aerogels are shown in Figure 2.7.

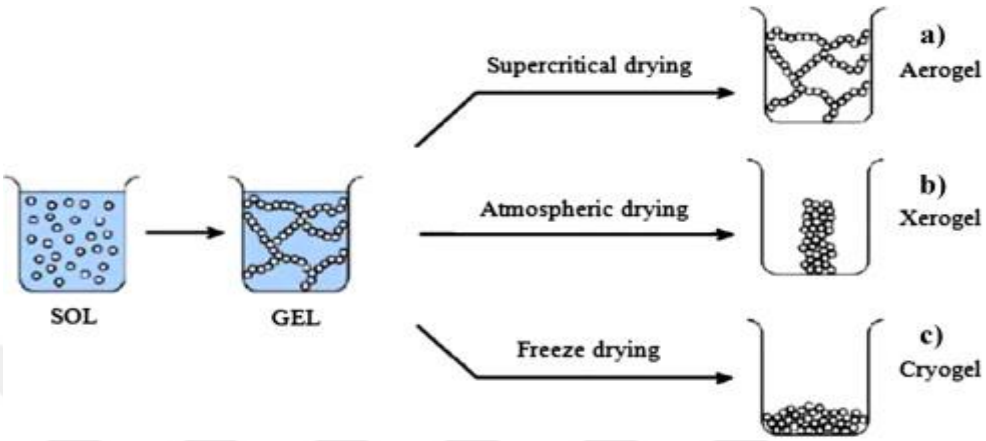

Figure 2.7: The basic scheme of synthesis of aerogels, xerogels, and cryogels [108].

Sol-Gel Process

This sol-gel process is chemically related to an organic polycondensation reaction in which small molecules form polymeric structures with the loss of substituents. Generally, the reaction results in a three-dimensional (3D) cross-linked network. The fact that small molecules are used as precursors for the formation of crosslinked materials includes several advantages, for example, the use of a solvent-based chemistry, which provides many advantages in the high control and processing of the purity and composition of the final product. The silicone-based sol-gel process is probably one of the most researched. For this reason, fundamental reaction principles are considered as a model system in this process. This also makes silicone-based sol-gel processes a widely used process for the synthesis of hybrid materials because of the organic groups being easily reacted using organic modified silanes. Si-C bonds are generally more resistant to hydrolysis reaction than metal-carbon bonds, so it is possible to easily connect a wide variety of organic groups to the formed network. Silica precursors are the starting materials of the sol-gel process. The synthesis begins with the hydrolysis of suitable precursor material mixed with water in a suitable solvent. The end point of condensation, which leads to hydrolysis reactions and a solid network, is accelerated by the addition of a catalyst. These reactions are seen in Figure 2.8. In the studies of Dorcheh and Abbasi, three different methods have been proposed, such as acid catalysis, base catalysis, and two-step acid-base catalysis

[82]. When silica aerogels were first synthesized, metallic precursors were used [85]. Currently, organic precursors such as TEOS, TMOS and some other silica-based precursors are preferred over metallic ones. These organic precursors have partial positive charges making them less susceptible to nucleophilic attack [109]. Also, since oxidation states are equal to coordination numbers, hydrolysis and condensation kinetics are slower than metal systems. To overcome these slow kinetics, acid or base catalysts are often added to the solution. Therefore, the pH used generally influences the kinetics expressed by the gel point of the sol-gel reaction.

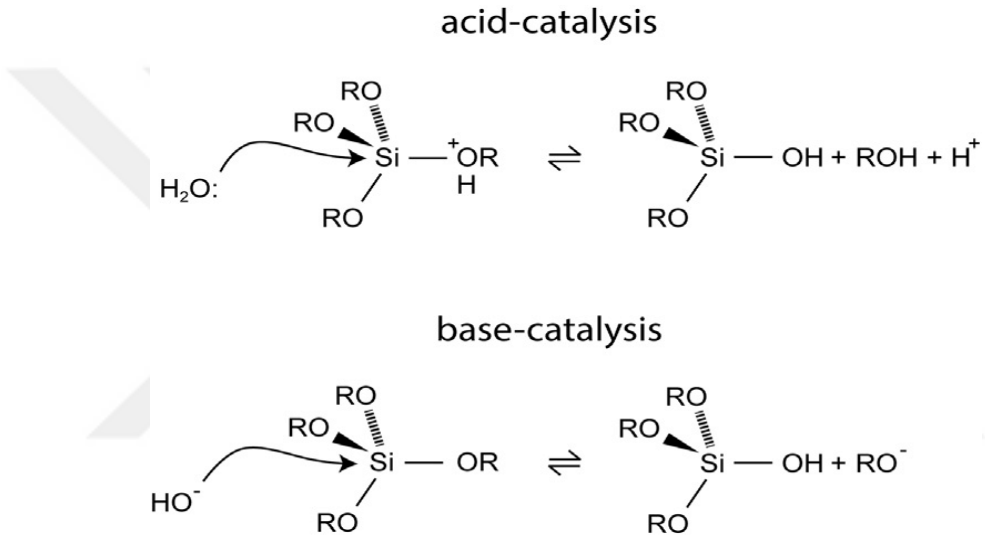

Figure 2.8: Acid and base catalysis of silicone-based sol-gel process [110].

The reaction is the slowest at the isoelectric point of the silica that is in between 2.5 and 4.5 depending on different parameters, and the rate increases rapidly by changing the pH. Reaction conditions have a strong influence not only on the kinetics of the reaction but also on the structure of the precursor materials. In general, larger substituents reduce reaction time due to steric inhibition. In addition, the substituents play a major role in the solubility of the starting material in the solvent. Moreover, water is prerequisite for the reaction, and if the organic substituents are large, the precursor usually becomes immiscible in the solvent. It is necessary to take into account that by changing the solvent, it can interfere with the hydrolysis reaction, for example, alcohols can undergo trans-esterification reactions, which lead to a rather complex balance in the mixture. Therefore, the reaction conditions must be fine-tuned for a well-defined end product. Furthermore, pH plays an important role not only in the mechanism, but also in the microstructure of

the final product. By applying acid-catalyzed reactions, an open network structure is formed in the first steps of this reaction, which then leads to condensation of small parts. On the other hand, the base catalyzed reaction leads to already highly cross-linked sol in the initial stages. Commonly used catalysts are HCl, NaOH or NH_4OH, but fluorides can also be used as catalysts which may lead to a rapid reaction time.

Hydrolysis

Hydrolysis is the first step in sol-gel synthesis. With the help of a catalyst, the alkoxide groups (-OR) of the -$Si(OR)_4$- organic precursor are replaced by hydroxyl groups (-OH) leading to the formation of individual silanol groups (Si-OH) [109]. The reverse reaction is called as esterification. The alkoxide group replaced by the precursor appears in the corresponding alcohol. Since water does not mix with alkoxysilanes due to the hydrophobicity of alkoxide groups, alcohols such as ethanol and methanol are also added to achieve miscibility between components. Thus, alcohols are used as co-solvents throughout the water to facilitate hydrolysis. It is carried out by adding an acid catalyst or a base catalyst as mentioned earlier. The rate and extent of hydrolysis depend on the strength and concentration of the catalyst as well as the temperature and the choice of solvent. Alkoxy groups tend to donate more electrons than hydroxyl groups, so as more alkoxy groups around the silicon atom are replaced by hydroxyl groups, the transition state becomes less stable and the rate of hydrolysis decreases. Additionally, bulky alkoxide groups have more impact on the rate of hydrolysis. Larger groups create more steric barriers and cause the reaction to be slower [111].

Condensation

Condensation reactions are polymerization reactions which lead to the formation of siloxane bonds (-Si-O-Si-) [111]. These reactions are classified into two different groups, such as condensation of water and alcohol molecules. Condensation reactions occur simultaneously with hydrolysis reactions. The condensation reaction rate depends on the steric effects such as hydrolysis. Less steric barrier in transition or intermediate molecules can contribute to the development of condensation kinetics; bulky groups reduce the rate of the reaction. Additionally, condensation reaction rates have a strong pH dependency. The pH of the reaction also affects the network structure as well as the rate of the reaction. Acid catalyzed reactions result in an open, highly purified structure, followed by

hydrolysis and condensation reactions. As a result of the base catalyzed reactions, a gel with larger pores is formed between the interconnected particles due to the higher condensation rate than hydrolysis. The result is the formation of dense particles in a condensed network. The dependence of the resulting gel structure on pH is shown in Figure 2.9. Both hydrolysis and condensation reactions are accelerated with low pH values. However, the rate of hydrolysis is higher than condensation reactions. As the pH gets higher, both reaction rates decrease.

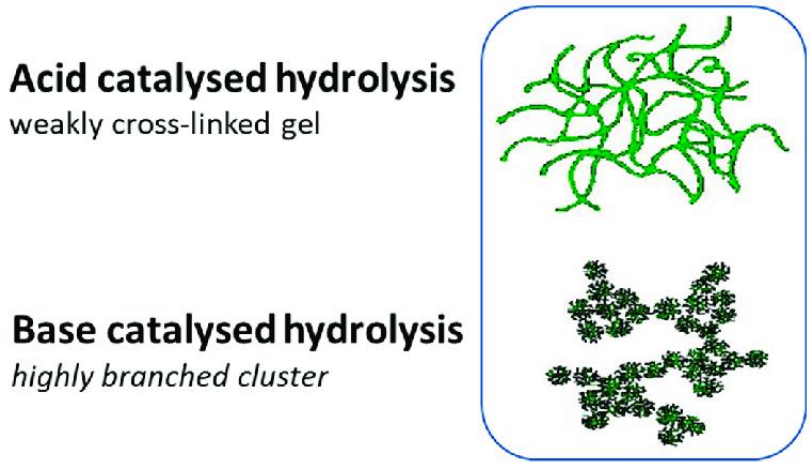

Figure 2.9: a) The gel structure of acid catalyzed hydrolysis reaction and b) the gel structure of base catalyzed hydrolysis reaction [112].

Gelation and Aging

The transition from a sol to a gel is defined as the gelation point, where the connections between the sol particles are formed to the extent that a solid containing internal pores in which the released alcohol is incorporated is obtained. However, at this point, the reaction is not over yet. Condensation reactions may continue for a long time until it reaches the final stage. Aging processes in which wet gels or alcohol gels are placed in suitable solutions are applied after the gelation step. The gelation time is considered as the time when the last bond is formed in the chains which forms the diffusion set. Condensation reactions do not stop after gelation occurs; it continues due to the flexible hydroxyl groups on the surface of the gels. Gelation can be considered as the final stage of condensation reactions with a sudden and large increase in viscosity. The gel is formed when the sol can carry an elastic stress. Thus, this process is called aging. During this reaction, the material shrinks and hardens [111]. Aging is carried out in the

drying process, where the material acquires a more compact structure and the corresponding crosslinking leads to increased hardness. During the drying process, large capillary forces of the porous evaporated liquids can lead to cracking of the materials. Drying rate, gelation time, pH, and similar reaction parameters can have a major impact on the cracking of the gels and should therefore be optimized. In some cases, damage to the gel network can lead to dust formation during the formation of the material, rather than monolithic parts. If the liquid in the pores is changed under supercritical conditions when the separation between liquid and vapor no longer exists, stress during the drying process can be prevented. This process results in high porous aerogels compared to conventionally dried xerogels. As various parameters affect the rate of the sol-gel reaction; if a homogeneous material is required, all parameters should be optimized. Optimization of all parameters is very essential in hybrid material synthesis. Therefore, undesired phase separations of organic and inorganic parts in materials weaken the properties of the material. It also weakens the properties of the leading materials that have not reacted with the network structure. This material is often visible even with the naked eye when it becomes opaque. Moreover, the water amount used, as well as the leading material ratio, is an important parameter in sol-gel reaction. If tetraalkoxysilanes are used as precursors, two water molecules are required per starting compound to form fully condensed SiO_2. Because using a lower H_2O/Si ratio will result in an alkoxide presence in the final product.

Drying Process

The liquid in the pores of gel is removed and replaced with air in the drying step. As the drying progresses, the gel structure becomes harder and stronger and eventually, shrinkage stops [111]. At this point, the liquid begins to withdraw to the porous structure of the gel. Due to the small pore size, surface tension and high capillary forces can form cracks at this stage of the process. The flow in the thin liquid film remaining on the pore walls continues, followed by evaporation and drying by direct evaporation through the pores. The liquid is then separated into parts and drying continues only with the evaporation of the liquid in the sample and the diffusion of the steam outside [109]. Therefore, different techniques should be used to remove pore fluid without damaging the structure. There are three types of drying techniques which are drying under ambient conditions, freeze drying and super critical drying.

Drying Under Ambient Conditions

Silica alcogels are dried at room temperature due to the high cost of other drying techniques. However, silica alcogels cannot withstand capillary pressure during evaporative drying and its structure will deteriorate. Therefore, silica alcogels should have a hydrophobic structure before the drying phase. Hydrogen atoms on the hydroxyl groups on the surface of silica alcohols are replaced with hydrophobic groups. Silicate agents such as hexamethyldisilazene (HMDZ), hexamethyldisiloxane (HMDS) [22], [113] and tetramethylchlorosilane (TMCS) [81] are used to make silica alcogels as hydrophobic. After the aging stage, the liquid in pores is replaced with a water-free solvent. Rao et al. showed that the physical and hydrophobic properties of hydrophobic silica aerogels dried at ambient pressure depend on the structure of the modifying solvent used during drying [22].

Freeze Drying

Freeze drying is a drying technique generally used to remove water or other solvents from a frozen product. Thus, this process is called as sublimation. Sublimation occurs when a solid frozen liquid turns directly into gas without turning into liquid phase. Pre-freezing, primary drying and secondary drying are three stages of the freeze drying. During the preliminary preparation, the sample must be completely frozen. Samples are cooled before freezing in a refrigerator or under liquid nitrogen. Small ice crystals are formed during rapid icing. Small ice crystals help to preserve the internal structure of the aerogel sample, but the frozen product obtained is more difficult to dry. As the rate of cooling decreases, the size of the ice crystals becomes larger. The temperature and pressure at which the solid content that needs to be removed is exalted should be adjusted. Thanks to the primary drying under low temperature and pressure, it results in a dry and structurally fine product. The chosen optimal temperature must both maintain the frozen sample and provide the maximum vapor pressure value of the sample, because the lower the temperature of sample, the longer the time required to complete the primary drying process. Moreover, vacuum pump is used in the freeze-drying system to reduce the pressure of the drying medium. A collection system consisting of a cold trap collects moisture from the frozen product. As a result, the collection system can remove all condensable gases, while the vacuum pump collects all other uncondensed gases. Secondary drying is essential to obtain completely dry sample and any residual moisture

that may still be present in the product must be removed. With this drying technique, the moisture attached is removed from the product [23].

Supercritical Drying

Although there are different techniques used for the drying of aerogels, supercritical drying is the most preferred drying method. It is preferred because there is no capillary tension that causes cracks in the aerogel resulting from drying. In this process, super critical carbon dioxide (sCO_2) reaches to aerogel pores and dissolves liquid in these pores. The liquid in the pores diffuses into the super critical liquid phase and thus, the capillary pressure due to the surface tension does not create any pressure on the aerogel structure. With this procedure, all liquid trapped in the pores is transferred to the supercritical liquid phase by diffusion without damaging the structure. Since alcohols have good solubility in CO_2, it is the most used gas in super critical drying processes. Moreover, as seen in Figure 2.10, CO_2 has critical conditions that are 31.04 ºC is the critical temperature and 7.39 MPa is the critical pressure [24]. In addition to this, CO_2 is a non-flammable, non-reactive and non-toxic gas. Thus, these properties of CO_2 make it a very useful and preferred gas for super critical drying process. In order to dry the liquid in the pores more efficiently, it is necessary to replace it with a water-free solvent as mentioned before, because the super critical CO_2 is insoluble in water and therefore cannot remove the liquid in the pores.

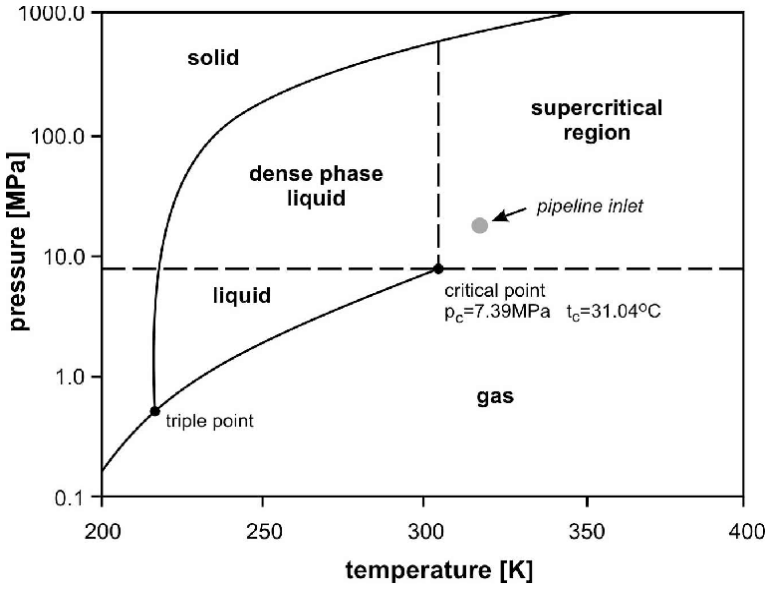

Figure 2.10: A phase diagram for CO_2 [114].

2.4.2 Applications of Aerogels

In this heading, the application areas of the aerogels regarding to the type of aerogel used, and the properties of the corresponding used aerogel will be discussed. Recently, the main application of aerogels is thermal insulation because aerogels are the best thermal insulating materials as well as vacuum insulation panels. However, other applications such as drug carrier and filling material in cosmetics, pharmacy, supercapacitor in electronics and absorber in environmental fields, or human health monitoring have already been developed [83], [94], [102], [115]–[118]. Some of common application areas of aerogels are summarized in the Table 2.4.

Table 2.4: Common applications of aerogels.

Application	**Type of aerogel**	**Properties of the corresponding aerogel**
Thermal insulation of buildings, pipelines, packaging, and textures	Silica, polyurethane, biopolymers, and carbon aerogels Composites: interlocking aerogel networks, aerogels containing clay	Thermal conductivity, high mechanical stability, and hydrophobicity
Cosmetics	Silica particles	Amorphous and potential in adsorbing liquids
Drug delivery	Biopolymers: alginate, pectin, starch, cellulose, and hybrids of these molecules	High surface area, accessibility of the pores of the drugs and surface modification and interest in specific drugs
Medical implants	Polyurea crosslinked aerogels, natural biopolymers: alginate,	Porous structure, biodegradability, and biocompatibility

	alginate-starch, gelatin hybrid materials	
Cherenkov detector	Silica	Refractive index
Space	Silica and hybrid materials	Transparency and thermal conductivity
Refinery	Resorcinol-formaldehyde and carbon	Porous and open pore structure
Construction materials	Silica	Mechanical properties and density of its composites
Absorbents for harmful gases	Silica, amino modified silica, graphene oxide	Surface functionalization and selectivity towards target molecules
Carrier materials for catalysts and electrocatalysis	SiO_2, various metal oxides, graphene oxide, Ru/graphene, gold, carbon (fuel cells), polysaccharides, (chitosan, alginate), noble metals, hybrids of semiconductor nanoparticles and photovoltaic materials	High surface area, stability in related gas or liquid phases, large mesoporous structure
Biocatalysts	Silica	Compatibility with enzymes and nontoxic byproducts during gelation
Tissue engineering	Biopolymers: alginate, pectin, starch, chitosan, cellulose, and their hybrid materials	Combination of mesoporous and macro porosity in the same material and biocompatibility
Ballistic protection	Crosslinked silica	Mechanical strength

Filling materials for dyes	Silica particles	Hydrophobicity and particle sizes
Energy and hydrogen storage devices	Carbon, graphene oxide, including those with functional pores	High surface area and conductivity
Sorbents for liquids, dangerous ions, oil leakage	Carbon, graphene oxide, including those with functional pores, combinations of functionalized and hydrophobized silica aerogels; magnetic cellulose aerogels, and clay aerogels	Surface functionalization, open porosity, hydrophobicity, and selectivity towards target molecules
Membranes	Carbon, fiber-aerogel hybrid materials, graphene, graphene oxide, chitosan	Selectivity towards target molecules, adjustment of pore sizes, and hydrophobicity

Applications of Graphene Aerogels Contributed to This Study

As the first application of synthesized graphene aerogel, we demonstrated the fabrication and application of a flexible piezotronics strain sensor architecture based on ZnO-NWs, embedded in graphene aerogel (GA). Flexible piezotronics strain sensors that are a very attractive tool for structural health monitoring applications and intelligent management. Their high sensitivity and fast response times makes them an ideal candidate for these applications, especially, the nanostructure architectures have become very intriguing to researchers [119], [120]. Various nano-architectures have been designed and fabricated from many different piezoelectric materials [121]. Among these piezoelectric materials, a large number of applications use ZnO nanomaterials, due to their unique advantages, such as biocompatibility, low cost, easy synthesis, and optical properties [122]–[124]. Especially ZnO, which received great attention after Wang's group ZnO nanowire based nanogenerator formation [121] that demonstrated excellent strain induced response properties. Thus, ZnO nanowires (ZnO-NWs) have become a center of attention in

building highly sensitive strain sensors. However, ZnO-NWs require compatible host materials that are electronically coupled with ZnO and allow flexible adaptive movements [125], [126]. Because, without the proper host material, ZnO-NWs can be very brittle and not suitable for flexible applications, especially under stress, ZnO layer is more prone to cracking and failure [126], [127]. Thus, ZnO-NWs are constantly embedded in various different materials to build flexible strain sensors, including different carbon fiber, carbon paper, and polymer composite materials. Subsequently, ZnO-NWs are embedded in synthesized graphene aerogel in this study.

As the second application of synthesized graphene aerogel, we demonstrated a new method to construct aerogel-based strain sensors that can effectively extract information from involuntary human motion. Since graphene aerogels (GA) were uniquely reinforced with carbon nanotubes (CNTs) to produce 3D hybrid frameworks, these frameworks provide stretchable characteristics, that the conductive pathways can be maintained under high strain or stress conditions. Maintaining the conductive pathways is very crucial to produce reliable information and it is one of the challenging problems for strain sensor designs. However, GA and CNTs mixture provides an excellent framework for reliable data gathering and their material functionalization properties provide great opportunity to produce sensitivity sensors. In this study, a strain sensor was prepared from highly functionalized GA and CNTs by reconstruction and dispersing technique, which is simple, low cost, and scalable. PDMS at silk composites were also embedded in GA/CNTs to achieve piezoelectric properties and produce a sensor that can be directly applied to the surface of the skin, while exhibiting high stretchability and sensitivity to subtle body motions [117].

Chapter 3:
MATERIALS & METHODS

In this chapter of thesis, experimental and characterization methods used in this study are covered. In the first part, procedure for graphene oxide, graphene aerogel synthesis and further synthesis methods for its applications are explained. In the second part, methods used to characterize the synthesized samples are described. In the final part, the measurement method of the *I-V* behavior of the strain sensor was investigated under static loading is described.

3.1 *Materials and Sample Preparation*

3.1.1 Materials

All the chemicals were used as they were received, and further purification was not done. Graphite (natural, 99.9995%), $NaNO_3$ (99%) were purchased from Alfa Aesar. H_2O_2 (30%) and H_2SO_4 (95-98%) were purchased from Merck Millipore. $KMnO_4$ acetone (≥99.5%), ethanol (99.9%), 2- propanol (≥99.5%) were obtained from Isolab. HCl (37%), NH_4OH (30%), ZnO (99.99%) powder and gold nanoparticles were purchased from Sigma Aldrich. Chemical reagents were analytical graded, and water was used as its deionized (DI) form.

3.1.2 Preparation of Graphene Oxide (GO) Solutions

In this study, modified Hummer's method was used to synthesize graphite oxide from graphite [7], [11]. The day before the synthesis, ice-cold H_2SO_4 and ice-cold distilled water were put into cubic container. Necessary chemicals were weighed and placed into little cups, then covered with paraffin. All the glass wares were cleaned by distilled water and placed to get dry. First, 138 mL of concentrated 98% H_2SO_4 was put into 1000 mL beaker onto 3 grams of $NaNO_3$ added and started stirring with 6 cm magnet. Then, ice bath was prepared by placing 4 big sized ice cubes to the corners of the box containing the reaction beaker. After, 3 grams of graphite was added after half an hour when temperature has dropped below 5 °C. It was crucial to keep temperature below 5 °C before the addition of $KMnO_4$ since it gives highly exothermic reactions. Then, 18 grams of $KMnO_4$ was added by little portions such as one pinch over a minute due to the drastic

increase in temperature may be observed. Thus, in order to control the temperature increase, it should be added when the temperature is below 5ºC. $KMnO_4$ addition took around 45 minutes. Then, the beaker was taken out from the ice bath one minute after the addition of $KMnO_4$ is done. Solution was left until its temperature reached to target temperature. Effervescence was observed due to vapors and then, beaker was placed to ice bath to get 18 ºC. Afterwards, the addition of 138 mL cold H_2O started, and it was added dropwise. As the temperature was raised slowly with the addition of distilled water, the solution was heated to 75ºC. This temperature should be maintained for 30 minutes. After it was kept at 75ºC for 30 minutes, 300 mL cold H_2O addition was started. In addition to this, 20 mL 30% H_2O_2 was added until yellow foam formation stopped. The resulting solution in powder form was washed third times with 5 wt.% HCl and then with distilled water. Later, this solution was separated and poured into centrifuge tubes and centrifuged for 10 minutes at 3000 rpm. Moreover, they were left overnight to obtain the exfoliation solutions. 0.3 grams of graphite oxide powder obtained was mixed with 100 mL of distilled water and put into ultrasonic bath for 4 hours. After ultrasonication was done, these solutions were required to be centrifuged for 30 minutes at 10000 rpm in order to eliminate the aggregated nanosheets. As a result of this synthesis process, graphene oxide solutions (GO) which are called for the exfoliation of graphene oxide nanosheets are obtained.

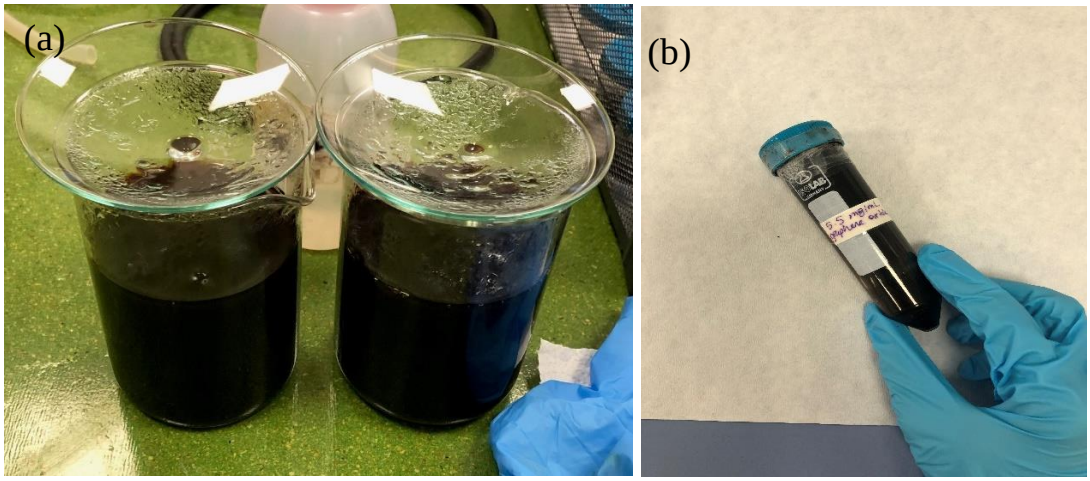

Figure 3.1: a) Obtained GO solutions by modified Hummer's method, b) 5.5 mg/mL concentrated GO solution.

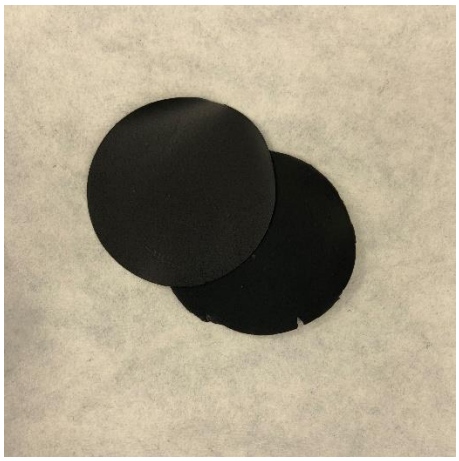

Figure 3.2: GO papers.

3.1.3 Preparation of Graphene Aerogel (GA)

GO was used as a precursor in this synthesis and it was synthesized as described in Section 3.1.2. Then, graphene aerogels (GAs) were synthesized by one-step hydrothermal reaction route. Since GO solution was used as a precursor, 2.5 mg/mL, 3.0 mg/mL and 5.5mg/mL of these solutions were taken separately and placed into autoclaves which are stainless steel and Teflon-lined. Then, it was put into a drying oven for 3 hours at 180 ºC. Consequently, it cooled down to room temperature and it was opened. Therefore, the hydrogel that is monolithic and black was formed. Later, it was put into distilled water to be purified and waited for 24 hours. This process was repeated for three times by changing its water content. After this procedure was done in three days, distilled water content of the hydrogel was exchanged with acetone and dried by (Speed SFE-15,000, Applied Separations, Inc.) supercritical CO_2 ($scCO_2$) drying method at 50 °C and 12.0 MPa. As a result, black monolithic formed GA was obtained as reported in [11], [128].

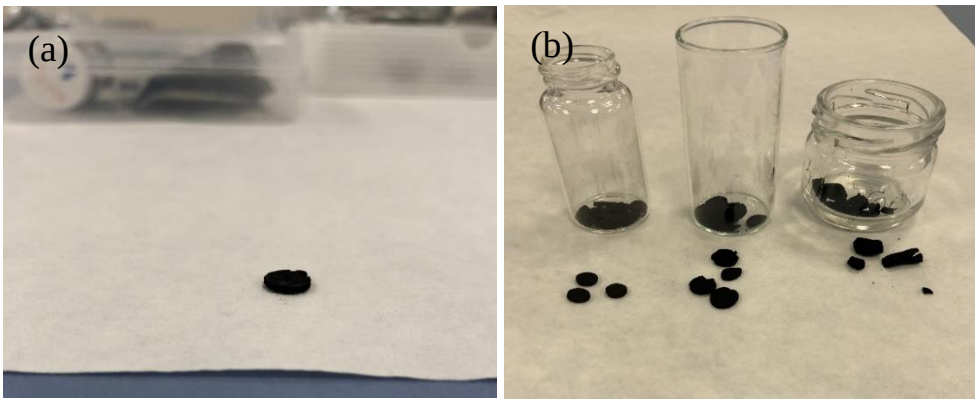

Figure 3.3: Obtained GA samples a) a piece of GA, b) GA samples obtained by different GO concentrations.

3.1.4 Synthesis and Growth of ZnO Nanowires embedded in GA

GO was synthesized as described in Section 3.1.2. Graphene aerogels were synthesized by the gelation of a graphene oxide (GO) suspension. GO was suspended (3.0 wt%) in deionized (DI) water and sonicated at 40 kHz. Then, in a glass vial, 5mL of the GO suspension was mixed with 500 μL of concentrated NH_4OH (30%). This solution was then transferred to a glass slide attached to rubber rectangular molds and cured in an oven at 80 °C for 72 hours. These resulting gels were removed from the molds and subjected to chemical exchange with acetone and deionized (DI) water, followed up by super critical CO_2 drying and pyrolyzed, carbonized, at 1000 °C under N_2 atmosphere for 3h [117], [129]. Resulted GA materials were then mixed with a ZnO nanoparticle solution (<100 nm) which was an important step to produce high quality ZnO-NW/GA interfaces, while ZnO nanowires were being synthesized with chemical vapor deposition (CVD) vapor trapping method. The final temperature of CVD was set to 600 ºC, 650 ºC, 700 ºC and 750 ºC. Among these temperatures, nanowire formations were obtained at 650 ºC. Finally, the whole device architecture was developed with contacts, Au for ZnO and Ag for GA, and encapsulated with polydimethylsiloxane (PDMS) elastomer that was essential to stabilize GA interconnected flakes [117].

Figure 3.4: Obtained samples via CVD at different temperatures.

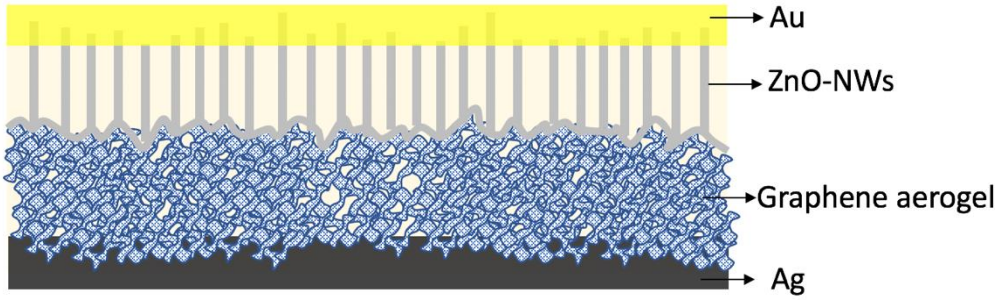

Figure 3.5: The schematic diagram ZnO-NWs embedded in GA piezotronics strain sensor.

Chemical Vapor Deposition (CVD)

Chemical vapor deposition (CVD) technique is used widely in processing of materials. The sample precursor is exposed to heat at high temperatures and under an atmosphere containing gas in this method. Then, the deposition of the precursor on the hot surface of substrate materials occurs because of the chemical reactions. Thus, a thin film layer formation is developed on the surface. Therefore, it allows to produce bulk materials or powders with a high product quality and synthetic diamonds, deposit materials on surface and develop composite materials. Since the parameters of CVD is controllable, it is possible to produce pure materials that are highly dense and uniform coating. Furthermore, surface morphology, orientation and crystal structures of the products are controlled by changing parameters as temperature and pressure during the process. Thus, this characteristic of CVD technique provides a wide usage area over several materials. On the other hand, this technique has some drawbacks as using toxic,

flammable, or explosive precursor that may cause chemical hazards. Also, vaporization rates are difficult to handle if more than one compound is present to be coated. Although this technique has some disadvantages as well as with its benefits, it is still a useful deposition method for solid materials [130]. In this study, OTF-1200X-S50-2F Mini CVD instrument was used to produce ZnO nanowires embedded in GA in section 3.1.4.

Figure 3.6: *OTF-1200X*-S50-2F mini *CVD* instrument.

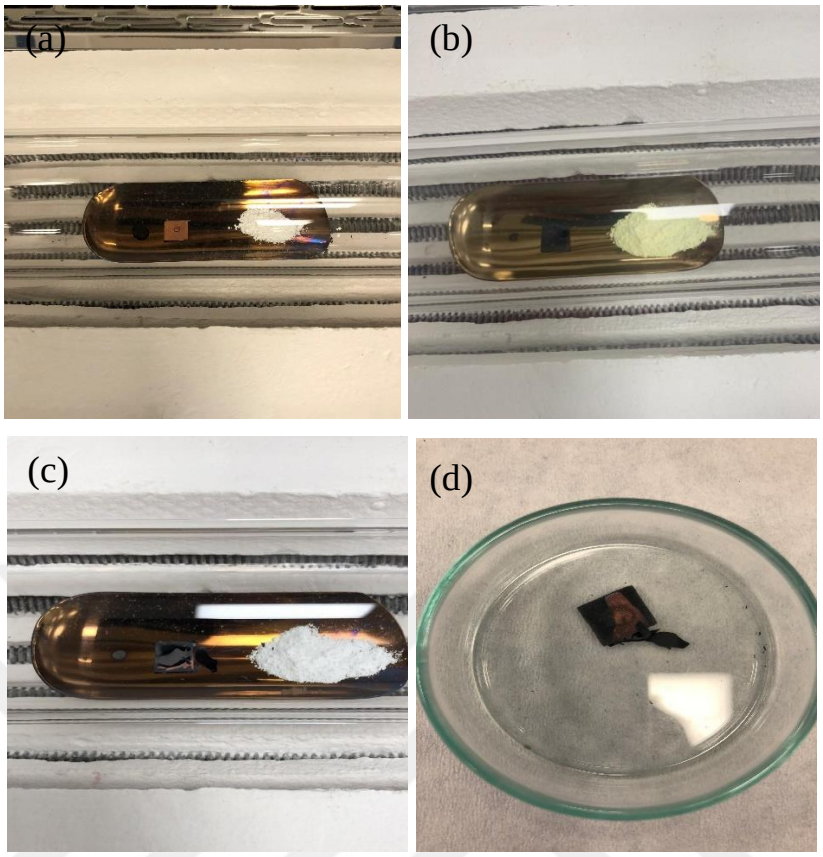

Figure 3.7: Synthesis of ZnO-NWs embedded in GA a) before synthesis, b) during synthesis, c) after synthesis, d) obtained sample after synthesis is done.

3.1.5 Reconstruction of Graphene Aerogel/Carbon Nanotubes (GA/CNTs) Synthesis

GA was synthesized by using precursor of GO solution that was synthesized in section 3.1.2, it was cross-linked via organic sol-gel chemistry as mentioned before in section 3.1.3, then it was followed by super critical drying and carbonization, which was achieved through pyrolysis at 1050 °C under N_2 atmosphere, as previously reported by [9], [10]. Resulted aerogel was then reconstructed and thus, it was grinded down via a vibrational ball while loading it with functionalized carbon nanotubes. Then, the solution was vacuum filtered and annealed at 600 °C. As a result, CNTs were produced a conformal coating on the surface of the GA with a pyramid shape as it can be seen in red dashed lines in Figure 3.8. The selective grinding and reconstruction were essential to form sufficient GA/CNTs interfaces, which is a very critical step to have a sensitive strain sensor [117].

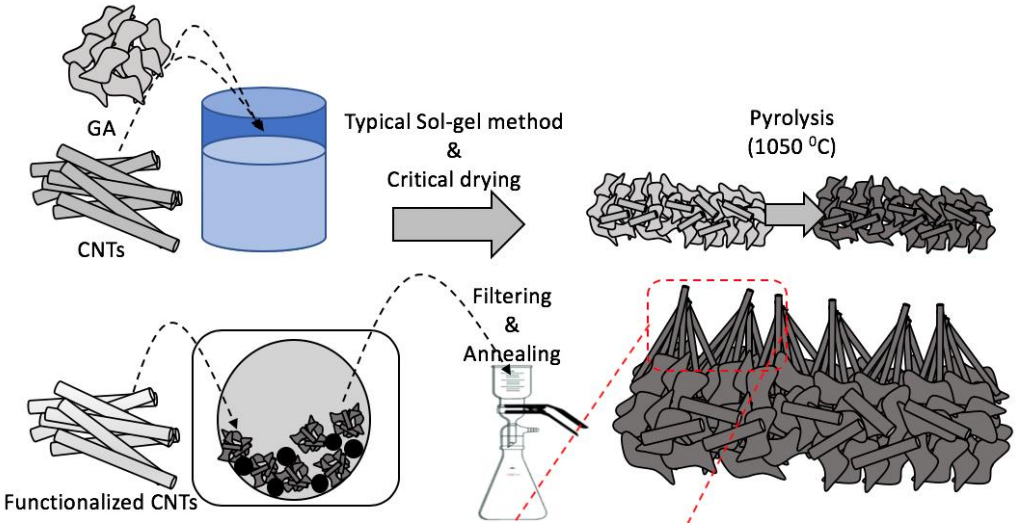

Figure 3.8: Schematic illustration of reconstructed GA/CNTs synthesis [117].

3.2 *Characterization Methods*

3.2.1 Raman Spectroscopy

Raman spectroscopy is a characterization technique which is not destructive and allows characterization of samples in structural and electronic environment. Its working principle is based on the inelastic scattering of photons. Thus, it causes excitation from ground state to an unstable state of molecules when sample gets exposed to light. There is not any energy exchange occurred during this method. Since the molecule gets excited, certain amount of energy is taken from photon but it is returned to ground state. Some intensity at a certain frequency is observed and this is a result of the difference occurred between the excited and ground states due to the scattered light. This is seen as a peak called Stokes band in Raman Spectroscopy. Some anti-Stokes bands are also observed because of the excited photons. On the other hand, anti-Stokes bands are existed at a higher frequency since excited molecules gives certain amount of energy to photon and scattering occurs from the sample. In addition to this, Stokes bands have higher intensity than anti-Stokes bands because of the large fraction. IR spectroscopy and Raman spectroscopy are complementary techniques to each other's. During vibration if molecule goes under a change in polarizability then it is called as Raman active. In IR spectroscopy, there is no observed vibrations for nonpolar molecules such as H_2, N_2 and O_2 whereas the stretch vibrations are obtained in Raman spectroscopy [131].

RAMAN spectra of GA samples were measured using Renishaw Invia Reflex Raman Microscope and Spectrometer in KUYTAM at a spectral resolution of 5 cm^{-1} using a visible excitation laser operating at 532 and 633 nm. Laser power was used at 5 mW. They were visualized with an integrated Leica microscope allowing confocal measurements using an objective.

3.2.2 X-Ray Diffraction (XRD)

To characterize crystalline materials in powder form, X-Ray Diffraction (XRD) spectroscopic method is used as a powerful and non-destructive technique. Analysis of crystalline structures, textural and structural properties and phase characteristics are done with the help of this method. Samples are diffracted at a specific angle from lattice planes and for this purpose, the generation of X-rays occurred by the heat given to a filament in the cathode ray tube. If this energy is sufficient to change positions of the electron located in the inner shell of the target sample, X-ray spectra is produced in a characteristic form for the corresponding sample [132]. X-ray diffraction patterns of synthesized GAs were measured by using XRD Bruker D8 Advance with CuKα radiation source. The 2θ range of the patterns was taken from 5 to 90°.

3.2.3 Field – Emission Scanning Electron Microscopy (FESEM)

Field - Emission scanning electron microscopy (FESEM) is a method which provides morphological and physical surface characteristics of the sample by scanning with focused electron beam that is high energy accelerated. The generation of the signals are the result of the interaction between sample and electron beam. Thus, they are produced as secondary electrons, photons, heat, backscattered electrons, and diffracted backscattered electrons. FESEM gives information about chemical compositions, topology, and crystalline structures of the samples analyzed [133]. In this study, FESEM analysis was performed by using a Zeiss Ultra Plus for imaging the synthesized GAs and synthesized nanowires embedded in graphene aerogel. Samples are carefully placed on the cell pasting with carbon tape. After the sample preparation, the cell was placed into the FESEM instrument under high vacuum to protect from any impurity that might be at the surface of samples.

3.3 *Measurement Method of Strain Sensor*

Strain is the compressive or tensile deformation in the shape of the materials. Thus, this occurs when any external force is applied. Strain gauge is a resistor which allows the measurement of the strain on the object. As the strain gauge is compressed or expanded, the electrical resistance changes. This change in resistance is measured in Wheatstone bridge which is an electrical circuit that allows to measure unknown resistance and thus, the corresponding current is obtained. In order to obtain I-V curve, different values of compression and expansion are applied to strain gauge [134]. Therefore, different strain values were applied in this study to obtain I-V behavior of strain sensor under static loading.

Chapter 4:
RESULTS & DISCUSSION

The characterization and measurements applied to the samples obtained as a result of the synthesis methods mentioned in the methods part and their results are discussed in this section. Synthesized GA must be dried via supercritical carbon dioxide reactor before characterization methods applied. For this reason, the produced graphene hydrogel was first dried to obtain GA and then the characterization methods were done. Moreover, ZnO nanowires embedded in GA and GA/CNTs were synthesized from the produced GA, for further applications of graphene aerogel. In the first part, for structural characterization of these samples, X-Ray Diffraction (XRD) and Raman Spectroscopy were used. In the second part of this part, Field - Emission scanning electron microscope (FESEM) was used for the morphological characterization of these samples. In the last part, according to electrical characterization done, electrical properties of GA based hybrid materials were discussed.

4.1 *Structural Characterization*

Crystal structural characterization of GO and GAs was carried by XRD (Bruker D8 Advance) with CuKα source. Raman (Renishaw Invia) with 532 and 633 nm laser were used to make defect analysis of GA structure. Porous structure of GA was analyzed by N_2 physisorption using surface area and porosimetry analyzer (Micromeritics ASAP 2020).

4.1.1 Structural Analysis by X-Ray Diffraction (XRD)

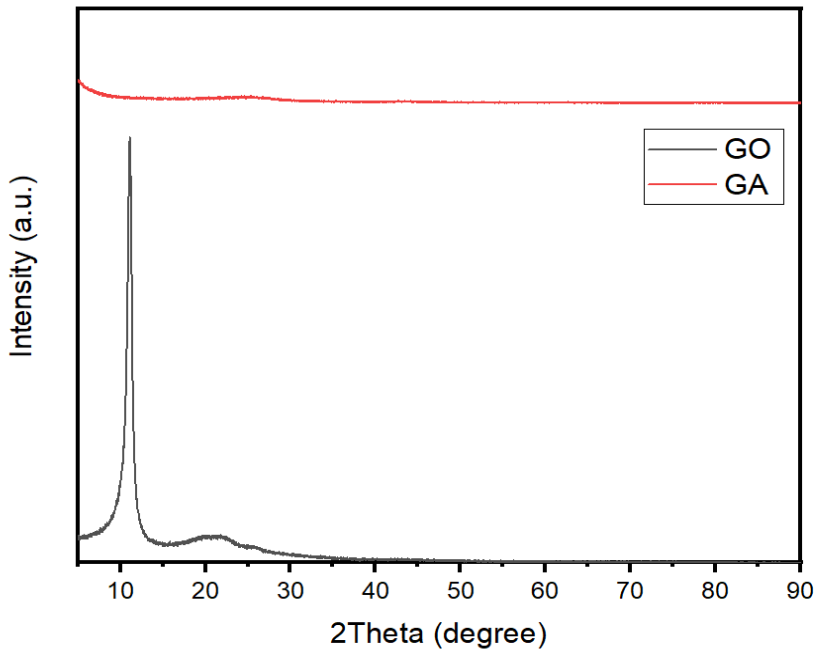

Figure 4.1: XRD diagram of synthesized GO and GA.

Figure 4.1 demonstrates XRD patterns for GO obtained after raw graphite powder going through the oxidation and exfoliation processes and GA resulted from this GO solution. It is reported as the XRD spectrum of graphite displays a strong characteristic (002) peak at $2\theta = 26°$. As it can be seen, this peak in the XRD pattern is vanished after the processes of oxidation and exfoliation done. Thus, a new sharp peak arises at 11° in the XRD spectrum of GO. Therefore, this confirms the conversion of graphite into GO because of the new peak corresponding to the lattice structure of GO. Finally, a broad peak at 23° is observed in the XRD spectrum of GA. All these patterns are reasonable with the previous results that are reported in [135].

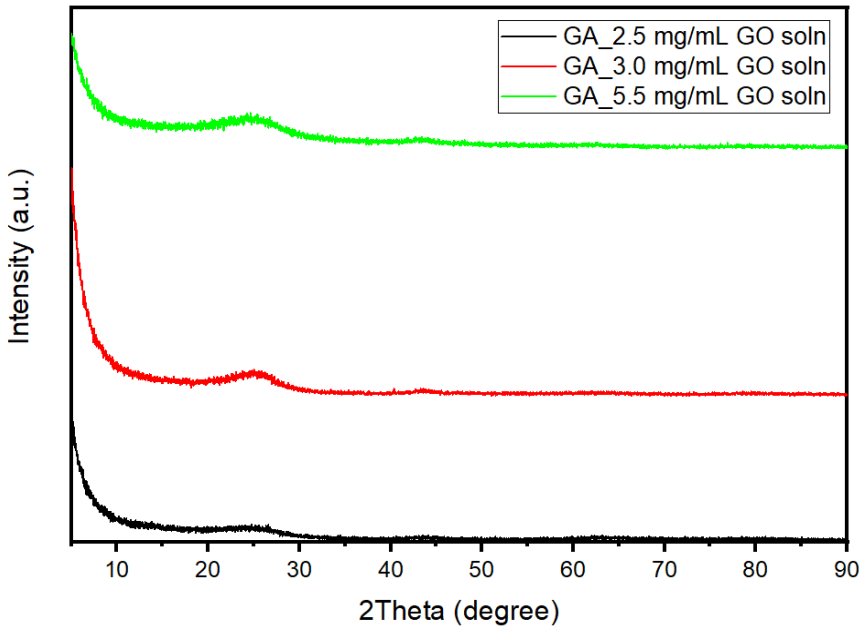

Figure 4.2: XRD diagram of GA based on different concentrated GO solutions.

In Figure 4.2, XRD patterns for GAs which were synthesized based on different concentrations GO solutions are demonstrated. Concentration of GO solutions were determined after the following of experimental process in Section 3.1.2. To determine, 5 mL of obtained GO solution was taken and filtered, then air dried. GO papers were taken from filter paper and then its mass was measured. Therefore, its mass was divided by the volume taken and as a result, its concentration in mg/mL was calculated for at least three times and the mean value of consistency taken. After the production of three different concentrated GO solutions that are 2.5 mg/mL, 3.0 mg/mL and 5.5 mg/mL respectively, corresponding GAs were produced. According to this XRD spectrum, broad peaks are lied at the similar position for all three samples. However, as concentrations increases, intensity of the peaks increases. This might be a result of the increase in surface area as the concentration increases [136]. Because the area where X-ray beam falls gets larger and this causes an increase in intensity. As a result, there is no obvious impurities observed as the concentration increases.

4.1.2 Structural Analysis by Raman Spectroscopy

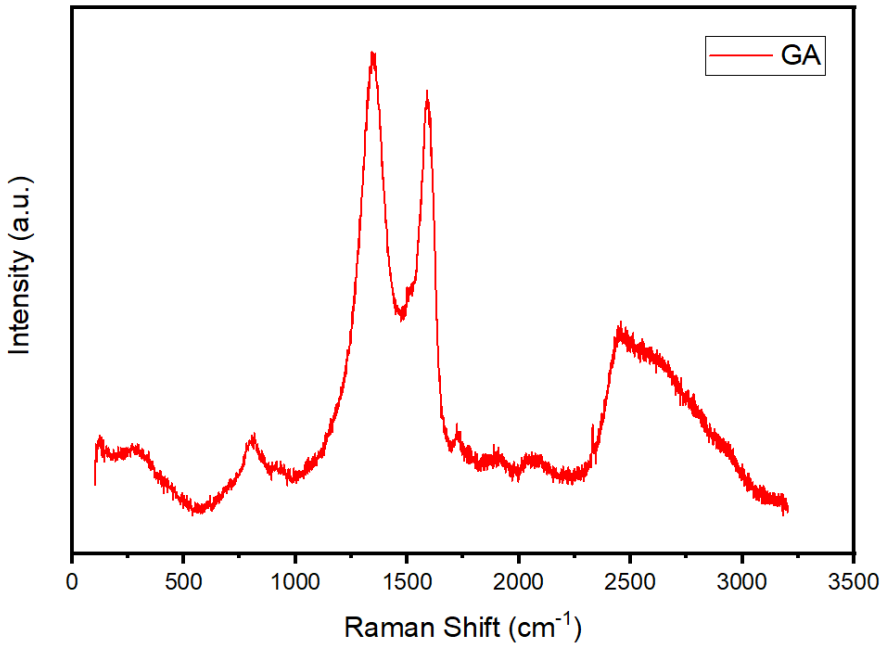

Figure 4.3: Raman Spectrum of GA.

Raman spectrum of GA is demonstrated in Figure 4.3. It is observed in GO spectrum that there are two main modes which are D mode and G mode in literature. D mode arises because of the presence of defects in hexagonal carbon network. Moreover, G mode occurs due to vibration in carbon-carbon bonds positioned in basal plane. 2D band is broader and much lower than G band that means there is multilayered graphene derivative structures. However, for the raman spectrum of GA, it is observed as D and 2D bands intensities are higher, thus this is believed to be a result of obtaining smaller pieces of graphene flakes due to longer ultrasonication treatment. Therefore, these smaller pieces cause more edges, and this enhances the intensity of D and 2D bands. Raman shifts for the observed D band is 1341 cm^{-1} and for G band 1589 cm^{-1} and for 2D band is 2697 cm^{-1}, respectively. Thus, these shifts are similar with the reported values in literature [136], [137].

4.1.3 Structural Analysis by N_2 adsorption/desorption isotherm

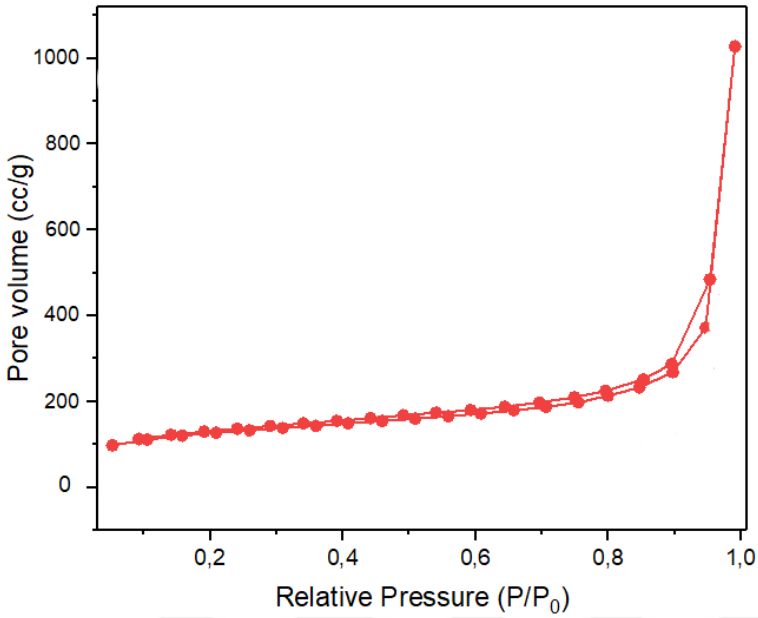

Figure 4.4: N_2 adsorption/desorption isotherm of produced GA.

BET (Branauer-Emmett-Teller) theory aims to investigate surface and pore characteristics of a porous material. The volume of gas adsorbed or desorbed on the solid surface is measured at constant temperature and different pressures [138]. By this way, one can obtain information about the surface area of the porous material, volume, and diameter of pores. Therefore, N_2 physisorption was used for this purpose. BET surface area of produced GA is 706 m^2/g, its pore volume is 1.48 cm^3/g with an average pore diameter of 5.6 nm. N_2 adsorption/desorption isotherm of produced GA is demonstrated in Figure 4.4. The nitrogen adsorption data demonstrates a Type IV isotherm. Thus, this isotherm indicates the presence of mesoporous characteristic as reported in [139].

4.2 *Morphological Characterization*

Surface morphology of GA was evaluated with FESEM (Zeiss Ultraplus) with accelerating voltage of 3.00 kV and probe of 200.0 nA. Morphological characterization was done for ZnO/GA nanowires and GA/CNTs with FESEM (Zeiss Ultraplus) with accelerating voltage of 10.00 kV and probe of 200.0 nA.

4.2.1 Morphological Analysis of Graphene Aerogel (GA) by Field – Emission Scanning Microscopy (FESEM)

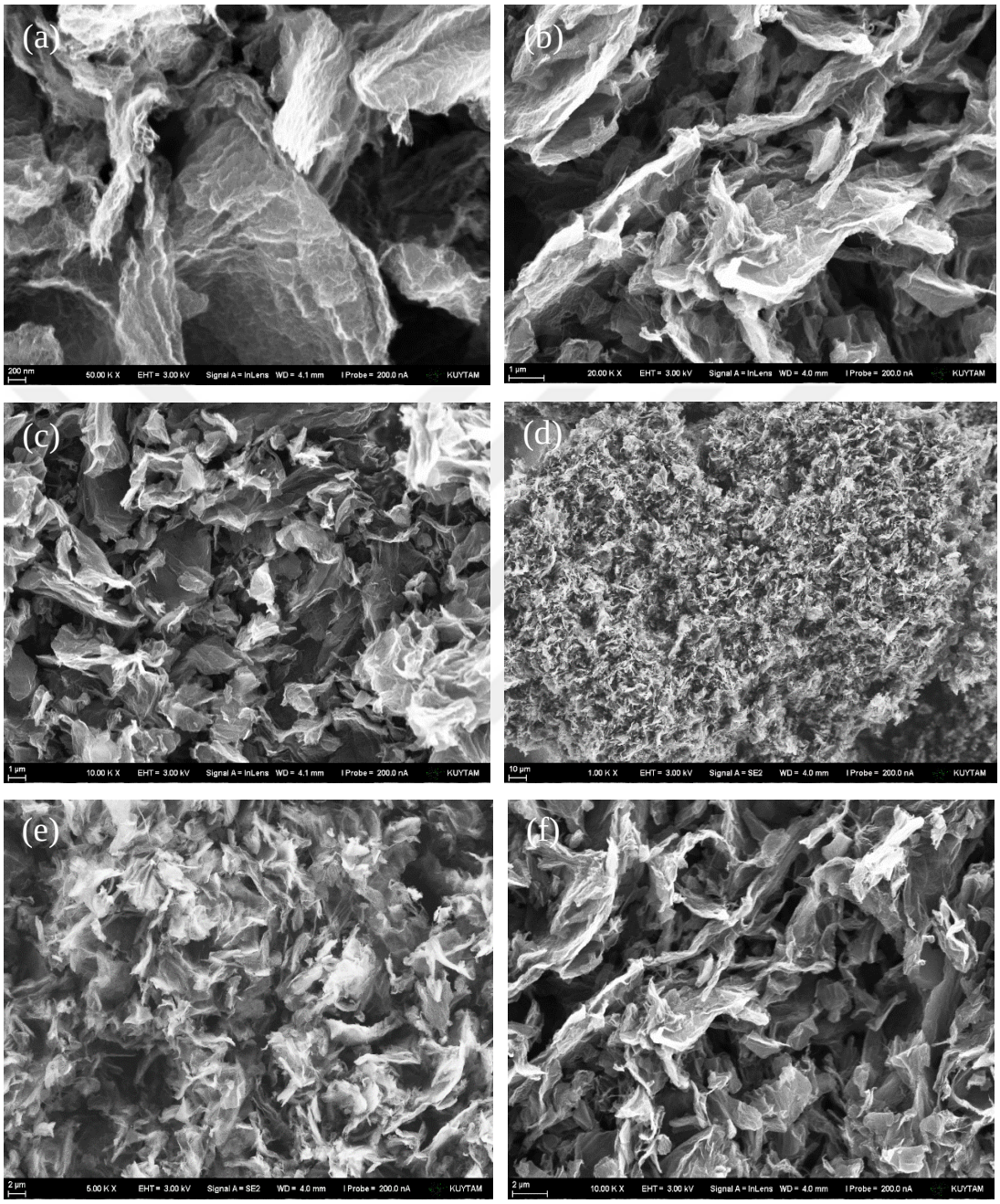

Figure 4.5: FESEM images of GA synthesized via modified Hummers method a-b) GA from 2.5 mg/mL concentration of GO solution, c-d) GA from 3.0 mg/mL solution, and e-f) GA from 5.5 mg/mL concentration of GO solution.

In order to study porous structures as internally and 3D networked of the synthesized graphene aerogels FESEM images are taken. Figure 4.5 shows a 3D network structure of graphene aerogel that is randomly oriented and it also forms sheetlike structures as seen

in Figure 4.5a,b which is similar to those reported previously. It can be obtained that these sheetlike structures have lateral dimensions and they are thin enough to pass electron beam. These images are representative for synthesized aerogels at different times via different concentrated GO solutions. It was obtained that the shapes of the aerogels are affected by the duration of hydrothermal treatment, pH used and concentrations used as they were reported in literature. Figure 4.5a is high magnified and Figure 4.5b-f images are low magnified. These two different magnifications are used in order to allow clear observations. GA structure is formed by randomly oriented rGOs that leave macropores between them. It is obvious that the voids lied in between nanosheets get narrowed as the hydrothermal treatment is carried on. The voids that indicates porousness are easily seen in Figure 4.5a,b. Nanosheets are observed as bent and twisted, creating many edges around. In addition to this, they are found as connected through their edges. These FESEM images are reasonable for the macroscopic properties of the monolithic structures demonstrated up to now [10], [11], [140]. As the graphene concentration increases, the graphene layer structure gradually crosslinks together to form a three-dimensional porous structure with different pore sizes. Meanwhile, the ability of graphene layers to crosslink becomes progressively evident with increasing concentration of graphene, so the size and density of the pores become smaller as shown in the FESEM images. Also, various natural folds occur on the graphene layers as the concentration increases.

4.2.2 Morphological Analysis of ZnO-NWs/GA by FESEM

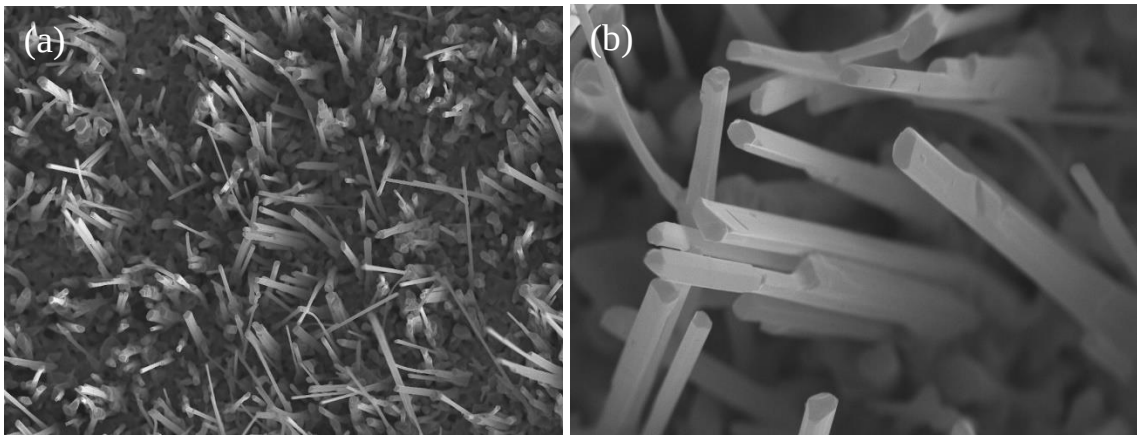

Figure 4.6: Top-view FESEM images of ZnO Nanowires fabricated by CVD method (a,b).

Figure 4.6a,b indicates the uniform growth of ZnO nanowires [141] throughout synthesized GA with a length of around 1 μm and average diameter of 30-35 nm. The growth of ZnO-NWs follows its surface topography due the non-flat nature of GA. Thus, this indicates that GA morphology was preserved after the growth of ZnO-NWs. This is also approved by the unchanged shape and volume of graphene aerogels before and after the growth of ZnO-NWs.

Figure 4.7: The cross-sectional FESEM image of the ZnO-NWs embedded in GA.

In Figure 4.7, it is seen that ZnO-NWs/GA structure is obtained upon the growth of ZnO nanowires embedded in synthesized graphene aerogel. The cross-sectional FESEM image of ZnO-NWs/GA also clearly shows that graphene aerogel is a good host material to accommodate ZnO-NWs, which commonly have cracking and adhesion problem during dynamic loading [142], [143]. GA enables continuous active contact to ZnO due to its flexibility and high porous structure.

4.2.3 Morphological Analysis of GA/CNTs by FESEM

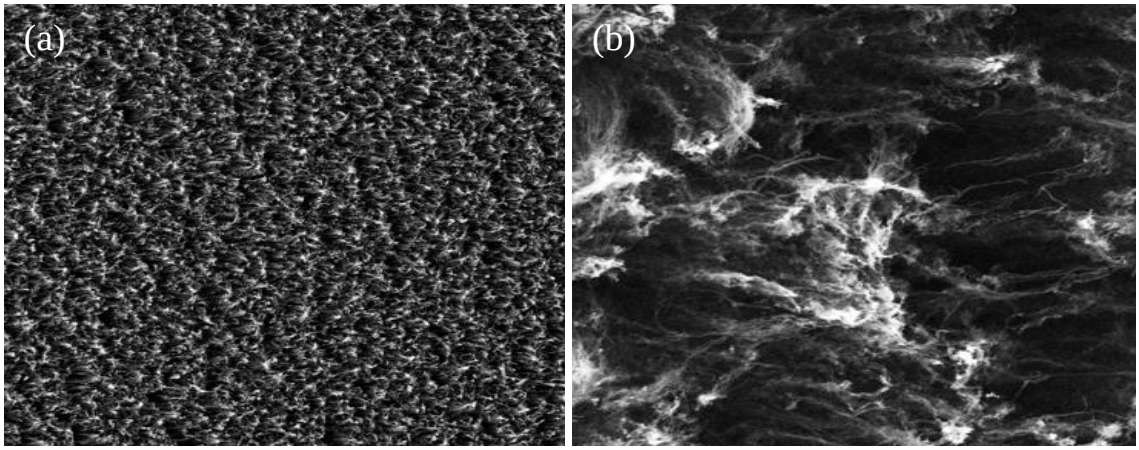

Figure 4.8: FESEM images of GA/CNTs a) top surface and b) CNT-assembly [117].

In figure 4.8a, top surface of the hybrid structure of GA/CNTs are illustrated. Figure 4.8b demonstrates the surface of the graphene aerogel, which has a conformal coating on, produced by CNTs with pyramidal shapes. The selective grinding and reconstruction are essential to form proper GA/CNTs interfaces. Thus, this is a very critical step to have a sensitive strain sensor that can respond at the end [117]. As these interfaces of GA/CNTs were obtained, they can be seen from the FESEM images.

4.3 *Electrical Characterization of GA Based Hybrid Materials*

4.3.1 Electrical Properties of ZnO/NWs Embedded in GA

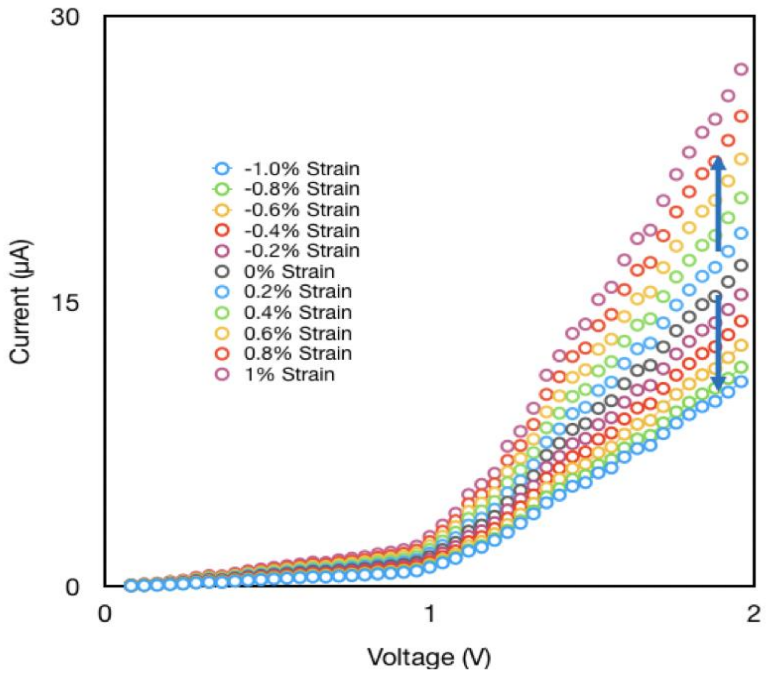

Figure 4.9: I-V characteristic of the strain sensor at different strains.

The characterization of the *I-V* behavior of the strain sensor was examined under the static loading shown in Figure 4.9. In different strains, Schottky barrier height (SBH) and current values in the revised curves change, shifting up and down with the pressure and strain, respectively.

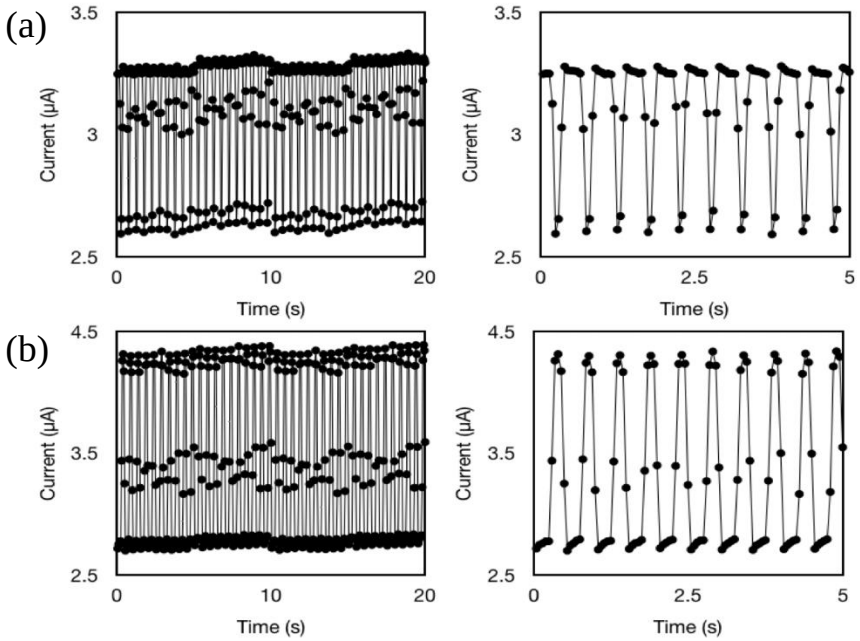

Figure 4.10: Current response of the strain sensor a) compressed, b) stretched at a frequency of 2 Hz under fixed bias 1.0 V.

The stability of the device was tested with many complete cycles of compressions and stretching repeated at a frequency of 2 Hz under a constant deviation of 1.0 V in Figure 4.10. It can be clearly seen that the current reaches approximately the same values in each cycle, demonstrating a stable behavior and desired electron transport behavior due to good Schottky junction formations [126], [144], [145].

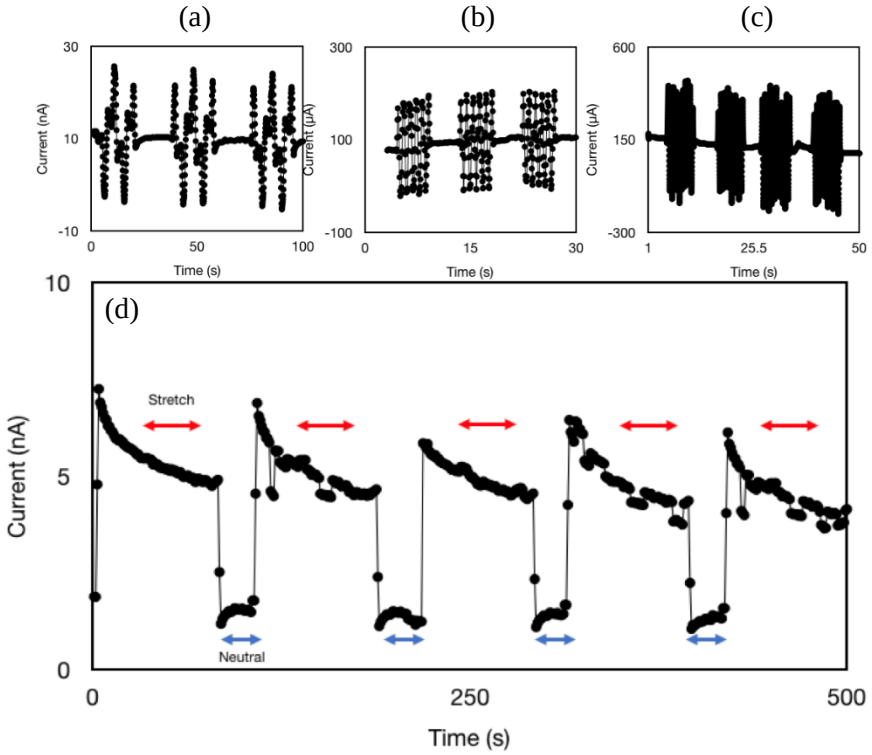

Figure 4.11: Dynamic response of the strain sensor at a frequency of a) 0.1, b) 1, and c) 2 Hz. d) time dependent piezo electric effect repeated cycle.

The response of the sensor was also examined under dynamic loading in Figure 4.11, measured at 0.1 Hz, 1.0 Hz and 2.0 Hz. As can be seen, the frequency of excitation follows the frequency of the response without deviation, and the amplitudes increase with the frequency, which shows high sensitivity for both tension and compression. Also, in Figure 4.11d, transient electron decay was tested in a fixed strain, strain sensors were stretched for 100 s and then repeatedly left for 10 s. It can be clearly seen that the strain sensor quickly returns to its initial conditions after the stretch has been recorded. The decay during hold is due to ZnO-NWs charge trapping behavior, which is commonly reported in the literature [146]. These results also clearly show that graphene aerogel is a good host material for ZnO-NWs.

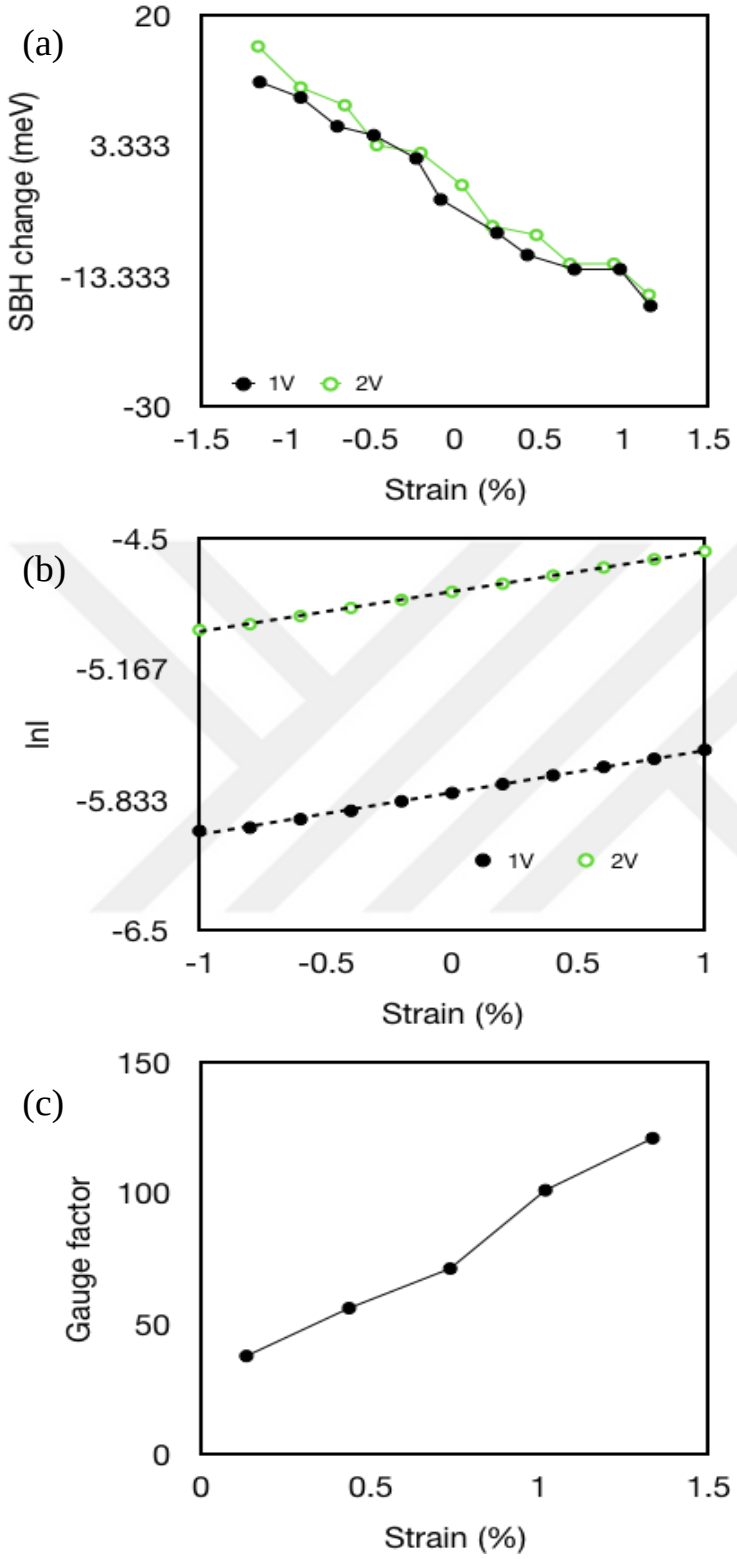

Figure 4.12: a) The derived change in SBH based on the thermionic emission–diffusion model, as a function of strain, b) Plot of In I vs. strain at a drain-source bias of 1.0 V and 2.0 V respectively, c) The plot of Gauge Factor (GF) vs. Strain (%).

Figure 4.12a shows the derived change in SBH based on the thermionic emission-diffusion model, as a function of strain at bias of 1.0 V and 2.0 V, with calculation method as in reference [121], [126]. In addition, logarithm plot of the current, at fixed bias of 1.0 V and 2.0 V, as a function of strain is linearly change with the applied strain, which is very consistent with previous reports [121], [125] and ensures the reliability of the device fabricated. To determine the performance of the strain sensor, gauge factor is calculated 120 by the equation of $GF = (\Delta R/R)/\Delta\varepsilon$, where R is the initial resistance, ΔR is the changed resistance, and $\Delta\varepsilon$ is the strain change in Figure 4.12c. This calculated value is much higher than the values reported for any ZnO/Carbon based strain sensors , 1.5 times higher than ZnO-Carbon nanofiber strain sensors (GF=81) [125] and almost 6 times higher than ZnO/paper [126] composite strain sensors (GF=21.12).

4.3.2 Electrical Properties of GA/CNTs Hybrid Materials

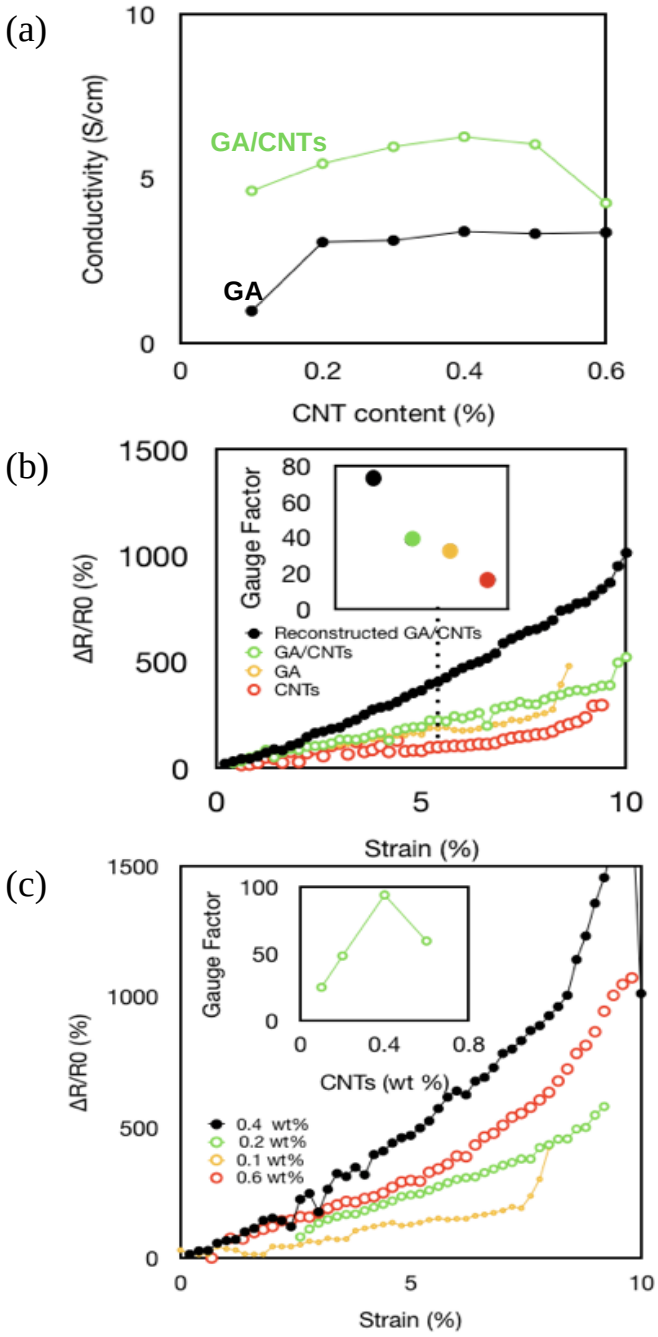

Figure 4.13: a) Electrical conductivity of GA/CNTs as a function of CNT content, b) ΔR/R0 vs. strain using different device architectures CNTs, GA, GA/CNTs, and Reconstructed GA/CNTs, Inset- gauge factor comparisons of these architectures c) ΔR/R0 vs. strain using different concentrations of CNTs on Reconstructed-GA/CNTs and Inset- effects of the CNT loading on gauge factor [117].

Figure 4.13a demonstrates the electrical conductivities of the hybrid structure that is GA/CNT. In literature, it has been reported as the concentration of GA increases, electrical conductivity of polymer increases by more than 10 orders of magnitude [147], [148]. Therefore, a similar trend is observed when CNT content is added to develop a hybrid structure. Thus, conductivity is enhanced by the addition of CNT. This loading results in more than 1.5 orders of magnitude improvement. However, saturation occurs due to further increase in CNT content beyond 0.44 wt %, whereas fractures and breakage occurs beyond 0.55 wt % in CNT content. Hence, electrical conductivity slightly degrades according to the literature [147], [149]. The variations in resistance, $\Delta R/R_0$ as a function of the applied strain under static loading was examined in Figure 4.13b-c. The relative change in resistance increases linearly with the applied strain until it fails. The gauge factor is obtained as the highest for the reconstructed GA/CNTs nanocomposite structure, which strongly indicates that the sensitivity of the sensor is directly related to the was the nanocomposite was prepared. Moreover, Gauge factor vs. CNT loading of reconstructed GA/CNTs shows a peak value of 94 with CNT concentration of 0.4 wt % in Figure 4.13b. The stress-strain curves of GA/CNTs also points a clear dependence on GA/CNT nanocomposite preparation and CNT loading. The reconstructed GA/CNTs demonstrate higher modulus, good elongation, and strength. In addition, due to the GA and CNT segregation, which is consistent with the above results, the crack propagation over 0.44 wt% by weight becomes dominant [117].

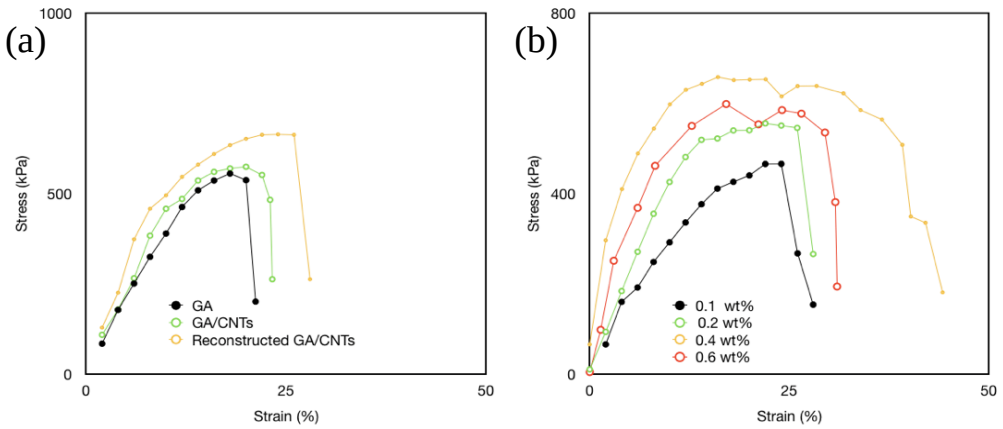

Figure 4.14: Stress vs. strain curves of GA/CNTs a) different GA architecture and b) different CNTs concentrations in reconstructed-GA/CNTs [117].

Figure 4.14 displays a typical stress-strain curves of different GA structures and different CNTs loadings of reconstructed GA/CNTs. Therefore, it is obvious that reconstructed GA/CNTs exhibits higher modulus, elongation, and strength compared to other geometries according to plots. In addition to this, the modulus of the reconstructed GA/CNTs increases with an increase in CNT concentration. On the other hand, it starts to decrease due to GA and CNT segregation beyond 0.5 wt % [117].

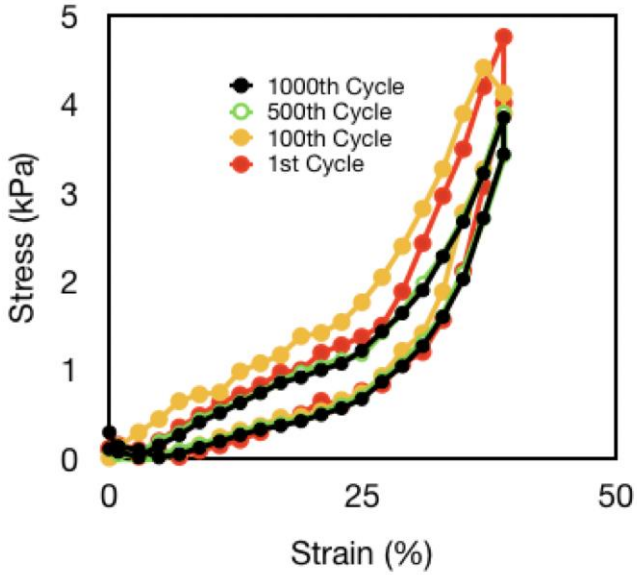

Figure 4.15: Cycling performance of reconstructed GA/CNTs [117].

The cyclic performance of reconstructed GA/CNTs was illustrated in Figure 4.15 as it displays linear characteristic at low strain values, then exhibits plateaus and exponential changes, in accordance with the literature [148], [150]. It can also be clearly seen that when GA/CNTs are released, the curve almost returns to its original position. This strongly demonstrates full recovery. In addition, it is apparent that reconstructed GA/CNTs show superior properties with minimal deformation implying their structural hardiness [117].

Chapter 5:
CONCLUSION & OUTLOOK

5.1 *Conclusion*

This dissertation is devoted to the synthesis of graphene aerogel for its applications based on strain sensors.

Throughout this thesis, studies on the production of graphene aerogel (GA) in order to use for its applications were conducted. Modified Hummer's method was used for the synthesis of graphene oxide solutions which are the precursor for the production of GA. For this purpose, graphene oxide solutions with different concentration were synthesized. Experiments were attempted with these GO solutions and stabilized to 3.0 mg/mL to use for further applications. Because as the amount of graphene oxide added increased, both impurities and active groups that might have remained on graphene reacted with the aerogel surface containing active groups might form new bonds. If the graphene oxide molecules cannot be distributed homogeneously, then this might cause undesired results as higher density, lower surface area or pore volume. The resulting hydrogels were dried via supercritical CO_2 drying to protect the branched mesopores that tend to settle if ambient drying is applied. After supercritical drying is utilized to obtain aerogels from hydrogels, hard and brittle aerogel samples were obtained rather than hydrogels that are sponge-like and soft features. Thus, the GA samples obtained are fragile like glass. The physicochemical characteristics of produced GA was analyzed by means of XRD and Raman Spectroscopy. The results revealed that high-quality monolithic black GAs were successfully obtained via hydrothermal treatment of GO solutions without any other additive. As a result, GAs with high specific surface areas (706 m^2/g) were successfully produced with an average pore diameter that is 5.6 nm. This improved surface area is much larger than most of those dried by freeze drying technique which were reported in the literature. Also, during the self-assembly of these GAs, deoxygenation took place simultaneously. In addition, while the GAs remained thermally stable under an inert atmosphere, the remaining oxygen functional groups were eliminated during heating. Conversely, they are completely decomposed at about 600 °C when heated under air. According to FESEM images, porous and randomly oriented 3D frameworks with thin layers of assembled graphene sheets were observed. The overlapping of these was

obtained as partially and resulted physical cross-linked areas that are wrinkled and folded on the surfaces of the stacked graphene layers.

GAs were later utilized as host material to develop a technique to produce flexible piezotronics strain sensor based on ZnO nanowires grown on graphene aerogel substrates. Graphene aerogels provide excellent receiving substrate properties that ZnO piezoelectric properties can be maintained under any strain conditions. *I-V* characteristic of the device demonstrates consistent SBH modulation and high sensitivity under static and dynamic loading. Moreover, it exhibits very good gauge factor, flexibility, and stability that indicates this device can be used for structural health monitoring of critical infrastructures, including highways, buildings, and pipelines. Thus, the results demonstrated that the produced GA is a proper host material for ZnO-NWs. Also, synthesis of GAs decorated with carbon nanotubes were produced to fabricate high precision and robust strain chemical sensors based on GA/CNT. The results show that the concentrations of CNT loading and GA reconstruction play an important role in adjusting the sensitivity of the sensor during fabrication. In addition, the synergy effect between GA and CNTs is crucial to achieve the desired electrical performance and gauge factor, especially during the stretch and hold cycles. Superior electrical conductivity, hardiness and stretchability can be obtained by proper CNT loading according to results obtained and published [117].

Overall, this thesis study exhibited a proper method to produce graphene aerogel combined with a versatile, unique, and low-cost methods to fabricate strain sensors based on produced GA for further applications. Furthermore, the development and characterization of a novel strain sensor based in the piezotronic effect was presented. The novelty of the device is related to the growth of ZnO nanowires over a layer of produced graphene aerogel. This device can also be used as an energy harvester to light up one LED. Moreover, reconstruction of GA/CNTs were demonstrated. These produced GA based hybrid materials can give insight into the future potential development of next-generation wearable electronic devices to monitor continuous human movement in real time.

5.2 *Suggestions*

Different methods of graphene oxide synthesis may further increase the efficiency of this synthesis, since it is possible to reach the reaction efficiency to 100 % with small fluctuations on the reaction values obtained by the investigations of publications on this subject. Further studies can be optimized to increase this produced amount with the same amount of materials used. Additionally, the effect of concentration changes in GO solutions, which resulted GA production, can be more examined by varying the concentrations. Three different concentration variations may not be enough to examine the effect of concentration on the production of GA, properly. The sensitivity of aerogel samples posed several obstacles throughout the production. With the innovations to be made in the drying system, the obstacles that occur during the production can be eliminated. Thus, conditions such as damaging the products while placing them in the system, damaging the products after being removed from the reactor after drying can be prevented. Due to pandemic, structural characterization part could not be focused deeply on this study. Thus, XPS and FTIR can be used as additional characterization methods for in-depth characterization of produced GAs. For the hybrid materials, structural characterization for both can be done to have knowledge on their chemical structures. Also, as it seemed that the density of the ZnO-NWs were very low, it might be better to provide FESEM images with higher magnification showing this or to work on the enhancement of the production method. The energy harvesting capability has not been investigated and characterized; thus, it can be a further study on this application. Moreover, different amount, type or composition of aerogel-based hybrid materials can be studied since there is a great challenge to fabricate high-performance flexible strain sensors with a conformal integration of the human body. Considering all the suggestions and results, it is possible to produce proper graphene aerogels and corresponding hybrid materials in laboratory scale appropriately with the further improvements for its applications.

BIBLIOGRAPHY

[1] Z. Li, Z. Liu, H. Sun, and C. Gao, “Superstructured Assembly of Nanocarbons: Fullerenes, Nanotubes, and Graphene,” *Chemical Reviews*. 2015, doi: 10.1021/acs.chemrev.5b00102.

[2] M. J. Allen, V. C. Tung, and R. B. Kaner, “Honeycomb carbon: A review of graphene,” *Chem. Rev.*, 2010, doi: 10.1021/cr900070d.

[3] F. Bonaccorso *et al.*, “Graphene, related two-dimensional crystals, and hybrid systems for energy conversion and storage,” *Science*. 2015, doi: 10.1126/science.1246501.

[4] K. S. Novoselov *et al.*, “Electric field in atomically thin carbon films,” *Science (80-.).*, 2004, doi: 10.1126/science.1102896.

[5] J. Hou, Y. Shao, M. W. Ellis, R. B. Moore, and B. Yi, “Graphene-based electrochemical energy conversion and storage: Fuel cells, supercapacitors and lithium ion batteries,” *Physical Chemistry Chemical Physics*. 2011, doi: 10.1039/c1cp21915d.

[6] O. C. Compton and S. T. Nguyen, “Graphene oxide, highly reduced graphene oxide, and graphene: Versatile building blocks for carbon-based materials,” *Small*. 2010, doi: 10.1002/smll.200901934.

[7] W. S. Hummers and R. E. Offeman, “Preparation of Graphitic Oxide,” *J. Am. Chem. Soc.*, 1958, doi: 10.1021/ja01539a017.

[8] G. Gorgolis and C. Galiotis, “Graphene aerogels: A review,” *2D Materials*. 2017, doi: 10.1088/2053-1583/aa7883.

[9] M. A. Worsley *et al.*, “Mechanically robust 3D graphene macroassembly with high surface area,” *Chem. Commun.*, 2012, doi: 10.1039/c2cc33979j.

[10] M. A. Worsley, P. J. Pauzauskie, T. Y. Olson, J. Biener, J. H. Satcher, and T. F. Baumann, “Synthesis of graphene aerogel with high electrical conductivity,” *J. Am. Chem. Soc.*, 2010, doi: 10.1021/ja1072299.

[11] F. E. Sarac Oztuna *et al.*, “Graphene Aerogel Supported Pt Electrocatalysts for Oxygen Reduction Reaction by Supercritical Deposition,” *Electrochim. Acta*, 2017, doi: 10.1016/j.electacta.2017.08.067.

[12] A. Krueger, *Carbon Materials and Nanotechnology*. 2010.

[13] F. Giubileo, A. Di Bartolomeo, L. Iemmo, G. Luongo, and F. Urban, “Field

emission from carbon nanostructures," *Applied Sciences (Switzerland)*. 2018, doi: 10.3390/app8040526.

[14] R. Sengupta, M. Bhattacharya, S. Bandyopadhyay, and A. K. Bhowmick, "A review on the mechanical and electrical properties of graphite and modified graphite reinforced polymer composites," *Progress in Polymer Science (Oxford)*. 2011, doi: 10.1016/j.progpolymsci.2010.11.003.

[15] S. Park and R. S. Ruoff, "Chemical methods for the production of graphenes," *Nat. Nanotechnol.*, 2009, doi: 10.1038/nnano.2009.58.

[16] S. Priyadarsini, S. Mohanty, S. Mukherjee, S. Basu, and M. Mishra, "Graphene and graphene oxide as nanomaterials for medicine and biology application," *J. Nanostructure Chem.*, 2018, doi: 10.1007/s40097-018-0265-6.

[17] C. Botas *et al.*, "Graphene materials with different structures prepared from the same graphite by the Hummers and Brodie methods," *Carbon N. Y.*, 2013, doi: 10.1016/j.carbon.2013.08.009.

[18] D. C. Marcano *et al.*, "Improved synthesis of graphene oxide," *ACS Nano*, 2010, doi: 10.1021/nn1006368.

[19] K. Tadyszak, J. K. Wychowaniec, and J. Litowczenko, "Biomedical applications of graphene-based structures," *Nanomaterials*. 2018, doi: 10.3390/nano8110944.

[20] C. J. Brinker and G. W. Scherer, *Sol-Gel Science: The Physics and Chemistry of Sol-Gel Processing*. 2013.

[21] R. Nandawar, S. Purnima, and Z. H. Fozia, "Synthesis and characterization of SiO2 nanoparticles by sol-gel process," *Indian J. Sci.*, vol. 1, no. 1, pp. 6–10, 2012, doi: 10.9734/ACSj/2014/10875.

[22] A. Parvathy Rao, G. M. Pajonk, and A. V. Rao, "Effect of preparation conditions on the physical and hydrophobic properties of two step processed ambient pressure dried silica aerogels," *J. Mater. Sci.*, 2005, doi: 10.1007/s10853-005-2853-3.

[23] Labconco, "A Guide To Freeze Drying for the Laboratory," *Ind. Serv. Publ.*, 2010, doi: 10.1017/CBO9781107415324.004.

[24] M. McHugh and V. Krukonis, *Supercritical Fluid Extraction: Principles and Practice*. 2013.

[25] Y. N. Kharzheev, "Use of silica aerogels in Cherenkov counters," *Phys. Part. Nucl.*, 2008, doi: 10.1134/s1063779608010085.

[26] B. Lang, “A LEED study of the deposition of carbon on platinum crystal surfaces,” *Surf. Sci.*, 1975, doi: 10.1016/0039-6028(75)90132-6.

[27] L. Xuekun, Y. Minfeng, H. Hui, and S. R. Rodney, “Tailoring graphite with the goal of achieving single sheets,” *Nanotechnology*, 1999.

[28] Y. Zhang, J. P. Small, W. V. Pontius, and P. Kim, “Fabrication and electric-field-dependent transport measurements of mesoscopic graphite devices,” *Appl. Phys. Lett.*, 2005, doi: 10.1063/1.1862334.

[29] A. A. Balandin *et al.*, “Superior thermal conductivity of single-layer graphene,” *Nano Lett.*, 2008, doi: 10.1021/nl0731872.

[30] H. P. Boehm, R. Setton, and E. Stumpp, “Nomenclature and terminology of graphite intercalation compounds (IUPAC Recommendations 1994),” *Pure Appl. Chem.*, 2007, doi: 10.1351/pac199466091893.

[31] A. Reina *et al.*, “Large area, few-layer graphene films on arbitrary substrates by chemical vapor deposition,” *Nano Lett.*, 2009, doi: 10.1021/nl801827v.

[32] L. H. Viculis, J. J. Mack, and R. B. Kaner, “A chemical route to carbon nanoscrolls,” *Science (80-.).*, 2003, doi: 10.1126/science.1078842.

[33] G. Xin, W. Hwang, N. Kim, S. M. Cho, and H. Chae, “A graphene sheet exfoliated with microwave irradiation and interlinked by carbon nanotubes for high-performance transparent flexible electrodes,” *Nanotechnology*, 2010, doi: 10.1088/0957-4484/21/40/405201.

[34] P. Sutter, “Epitaxial graphene: How silicon leaves the scene,” *Nat. Mater.*, 2009, doi: 10.1038/nmat2392.

[35] M. S. A. Bhuyan, M. N. Uddin, M. M. Islam, F. A. Bipasha, and S. S. Hossain, “Synthesis of graphene,” *Int. Nano Lett.*, 2016, doi: 10.1007/s40089-015-0176-1.

[36] G. Eda and M. Chhowalla, “Chemically derived graphene oxide: Towards large-area thin-film electronics and optoelectronics,” *Advanced Materials*. 2010, doi: 10.1002/adma.200903689.

[37] B. C. Brodie, “XXIII. - Researches on the atomic weight of graphite,” *Q. J. Chem. Soc. London*, 1860, doi: 10.1039/QJ8601200261.

[38] S. Pei and H. M. Cheng, “The reduction of graphene oxide,” *Carbon N. Y.*, 2012, doi: 10.1016/j.carbon.2011.11.010.

[39] S. Mao, H. Pu, and J. Chen, “Graphene oxide and its reduction: Modeling and experimental progress,” *RSC Advances*. 2012, doi: 10.1039/c2ra00663d.

[40] L. Staudenmaier, “Verfahren zur Darstellung der Graphitsäure,” *Berichte der Dtsch. Chem. Gesellschaft*, 1898, doi: 10.1002/cber.18980310237.

[41] M. Cai, D. Thorpe, D. H. Adamson, and H. C. Schniepp, “Methods of graphite exfoliation,” *Journal of Materials Chemistry*. 2012, doi: 10.1039/c2jm34517j.

[42] Y. Si and E. T. Samulski, “Synthesis of water soluble graphene,” *Nano Lett.*, 2008, doi: 10.1021/nl080604h.

[43] J. I. Paredes, S. Villar-Rodil, A. Martínez-Alonso, and J. M. D. Tascón, “Graphene oxide dispersions in organic solvents,” *Langmuir*, 2008, doi: 10.1021/la801744a.

[44] M. J. McAllister *et al.*, “Single sheet functionalized graphene by oxidation and thermal expansion of graphite,” *Chem. Mater.*, 2007, doi: 10.1021/cm0630800.

[45] C. Mattevi *et al.*, “Evolution of electrical, chemical, and structural properties of transparent and conducting chemically derived graphene thin films,” *Adv. Funct. Mater.*, 2009, doi: 10.1002/adfm.200900166.

[46] X. Wang, L. Zhi, and K. Müllen, “Transparent, conductive graphene electrodes for dye-sensitized solar cells,” *Nano Lett.*, 2008, doi: 10.1021/nl072838r.

[47] L. Huang, Y. Liu, L. C. Ji, Y. Q. Xie, T. Wang, and W. Z. Shi, “Pulsed laser assisted reduction of graphene oxide,” *Carbon N. Y.*, 2011, doi: 10.1016/j.carbon.2011.01.067.

[48] W. Chen, L. Yan, and P. R. Bangal, “Preparation of graphene by the rapid and mild thermal reduction of graphene oxide induced by microwaves,” *Carbon N. Y.*, 2010, doi: 10.1016/j.carbon.2009.11.037.

[49] S. Stankovich *et al.*, “Synthesis of graphene-based nanosheets via chemical reduction of exfoliated graphite oxide,” *Carbon N. Y.*, 2007, doi: 10.1016/j.carbon.2007.02.034.

[50] T. Kuila, A. K. Mishra, P. Khanra, N. H. Kim, and J. H. Lee, “Recent advances in the efficient reduction of graphene oxide and its application as energy storage electrode materials,” *Nanoscale*. 2013, doi: 10.1039/c2nr32703a.

[51] L. J. Cote, R. Cruz-Silva, and J. Huang, “Flash reduction and patterning of graphite oxide and its polymer composite,” *J. Am. Chem. Soc.*, 2009, doi: 10.1021/ja902348k.

[52] Y. H. Ng, A. Iwase, A. Kudo, and R. Amal, “Reducing graphene oxide on a visible-light BiVO4 photocatalyst for an enhanced photoelectrochemical water

splitting," *J. Phys. Chem. Lett.*, 2010, doi: 10.1021/jz100978u.

[53] Y. H. Ding, P. Zhang, Q. Zhuo, H. M. Ren, Z. M. Yang, and Y. Jiang, "A green approach to the synthesis of reduced graphene oxide nanosheets under UV irradiation," *Nanotechnology*, 2011, doi: 10.1088/0957-4484/22/21/215601.

[54] V. B. Mohan, R. Brown, K. Jayaraman, and D. Bhattacharyya, "Characterisation of reduced graphene oxide: Effects of reduction variables on electrical conductivity," *Mater. Sci. Eng. B Solid-State Mater. Adv. Technol.*, 2015, doi: 10.1016/j.mseb.2014.11.002.

[55] Y. Chen *et al.*, "Reduced graphene oxide films with ultrahigh conductivity as Li-ion battery current collectors," *Nano Lett.*, 2016, doi: 10.1021/acs.nanolett.6b00743.

[56] W. Park, J. Hu, L. A. Jauregui, X. Ruan, and Y. P. Chen, "Electrical and thermal conductivities of reduced graphene oxide/polystyrene composites," *Appl. Phys. Lett.*, 2014, doi: 10.1063/1.4869026.

[57] X. Zeng, J. Yang, L. Zhang, L. Chen, and W. Yuan, "Homogeneous dispersion of high-conductive reduced graphene oxide sheets for polymethylmethacrylate nanocomposites," *Powder Diffr.*, 2014, doi: 10.1017/S0885715614000050.

[58] S. Stankovich *et al.*, "Graphene-based composite materials," *Nature*, 2006, doi: 10.1038/nature04969.

[59] P. G. Ren, D. X. Yan, X. Ji, T. Chen, and Z. M. Li, "Temperature dependence of grapheme oxide reduced by hydrazine hydrate," *Nanotechnology*, 2011, doi: 10.1088/0957-4484/22/5/055705.

[60] X. Zhou, J. Zheng, H. Wu, H. Yang, J. Zhang, and S. Guo, "Reducing graphene oxide via hydroxylamine: A simple and efficient route to graphene," *J. Phys. Chem. C*, 2011, doi: 10.1021/jp202575j.

[61] Y. Chen, X. Zhang, P. Yu, and Y. Ma, "Stable dispersions of graphene and highly conducting graphene films: A new approach to creating colloids of graphene monolayers," *Chem. Commun.*, 2009, doi: 10.1039/b907723e.

[62] T. Zhou *et al.*, "A simple and efficient method to prepare graphene by reduction of graphite oxide with sodium hydrosulfite," *Nanotechnology*, 2011, doi: 10.1088/0957-4484/22/4/045704.

[63] V. H. Pham *et al.*, "Chemical functionalization of graphene sheets by solvothermal reduction of a graphene oxide suspension in N-methyl-2-

pyrrolidone," *J. Mater. Chem.*, 2011, doi: 10.1039/c0jm02790a.

[64] Z. J. Fan *et al.*, "Facile synthesis of graphene nanosheets via fe reduction of exfoliated graphite oxide," *ACS Nano*, 2011, doi: 10.1021/nn102339t.

[65] Z. Fan, K. Wang, T. Wei, J. Yan, L. Song, and B. Shao, "An environmentally friendly and efficient route for the reduction of graphene oxide by aluminum powder," *Carbon*. 2010, doi: 10.1016/j.carbon.2009.12.063.

[66] R. S. Dey, S. Hajra, R. K. Sahu, C. R. Raj, and M. K. Panigrahi, "A rapid room temperature chemical route for the synthesis of graphene: Metal-mediated reduction of graphene oxide," *Chem. Commun.*, 2012, doi: 10.1039/c2cc16031e.

[67] X. Mei and J. Ouyang, "Ultrasonication-assisted ultrafast reduction of graphene oxide by zinc powder at room temperature," *Carbon N. Y.*, 2011, doi: 10.1016/j.carbon.2011.08.019.

[68] S. Pei, J. Zhao, J. Du, W. Ren, and H. M. Cheng, "Direct reduction of graphene oxide films into highly conductive and flexible graphene films by hydrohalic acids," *Carbon N. Y.*, 2010, doi: 10.1016/j.carbon.2010.08.006.

[69] I. K. Moon, J. Lee, R. S. Ruoff, and H. Lee, "Reduced graphene oxide by chemical graphitization," *Nat. Commun.*, 2010, doi: 10.1038/ncomms1067.

[70] J. Zhang, H. Yang, G. Shen, P. Cheng, J. Zhang, and S. Guo, "Reduction of graphene oxide vial-ascorbic acid," *Chem. Commun.*, 2010, doi: 10.1039/b917705a.

[71] M. J. Fernández-Merino *et al.*, "Vitamin C is an ideal substitute for hydrazine in the reduction of graphene oxide suspensions," *J. Phys. Chem. C*, 2010, doi: 10.1021/jp100603h.

[72] D. Chen, L. Li, and L. Guo, "An environment-friendly preparation of reduced graphene oxide nanosheets via amino acid," *Nanotechnology*, 2011, doi: 10.1088/0957-4484/22/32/325601.

[73] Y. K. Kim, M. H. Kim, and D. H. Min, "Biocompatible reduced graphene oxide prepared by using dextran as a multifunctional reducing agent," *Chem. Commun.*, 2011, doi: 10.1039/c0cc05005a.

[74] Y. Lei, Z. Tang, R. Liao, and B. Guo, "Hydrolysable tannin as environmentally friendly reducer and stabilizer for graphene oxide," *Green Chem.*, 2011, doi: 10.1039/c1gc15081b.

[75] C. Vallés, J. David Núñez, A. M. Benito, and W. K. Maser, "Flexible conductive

graphene paper obtained by direct and gentle annealing of graphene oxide paper," *Carbon N. Y.*, 2012, doi: 10.1016/j.carbon.2011.09.042.

[76] O. K. Park *et al.*, "In situ synthesis of thermochemically reduced graphene oxide conducting nanocomposites," *Nano Lett.*, 2012, doi: 10.1021/nl203803d.

[77] H. L. Guo, X. F. Wang, Q. Y. Qian, F. Bin Wang, and X. H. Xia, "A green approach to the synthesis of graphene nanosheets," *ACS Nano*, 2009, doi: 10.1021/nn900227d.

[78] G. Kickelbick, "Introduction to Hybrid Materials," *Hybrid Materials: Synthesis, Characterization, and Applications*. 2007, doi: 10.1002/9783527610495.ch1.

[79] A. C. Pierre, "History of Aerogels," in *Aerogels Handbook*, 2011.

[80] D. A. Loy, "Sol-Gel Processing of Hybrid Organic-Inorganic Materials Based on Polysilsesquioxanes," in *Hybrid Materials: Synthesis, Characterization, and Applications*, 2007.

[81] A. Soleimani Dorcheh and M. H. Abbasi, "Silica aerogel; synthesis, properties and characterization," *Journal of Materials Processing Technology*. 2008, doi: 10.1016/j.jmatprotec.2007.10.060.

[82] *Ullmann's Encyclopedia of Industrial Chemistry*. 2000.

[83] L. W. Hrubesh, "Aerogel applications," *J. Non. Cryst. Solids*, 1998, doi: 10.1016/S0022-3093(98)00135-5.

[84] I. Smirnova and P. Gurikov, "Aerogels in chemical engineering: Strategies toward tailor-made aerogels," *Annual Review of Chemical and Biomolecular Engineering*. 2017, doi: 10.1146/annurev-chembioeng-060816-101458.

[85] S. S. Kistler, "Coherent expanded aerogels," *J. Phys. Chem.*, 1932, doi: 10.1021/j150331a003.

[86] K. Tajiri, K. Igarashi, and T. Nishio, "Effects of supercritical drying media on structure and properties of silica aerogel," *J. Non. Cryst. Solids*, 1995, doi: 10.1016/0022-3093(95)00038-0.

[87] N. Leventis, A. Palczer, L. McCorkle, G. Zhang, and C. Sotiriou-Leventis, "Nanoengineered silica-polymer composite aerogels with No need for supercritical fluid drying," *J. Sol-Gel Sci. Technol.*, 2005, doi: 10.1007/s10971-005-1372-7.

[88] L. A. Capadona, M. A. B. Meador, A. Alunni, E. F. Fabrizio, P. Vassilaras, and N. Leventis, "Flexible, low-density polymer crosslinked silica aerogels," *Polymer*

(Guildf)., 2006, doi: 10.1016/j.polymer.2006.05.073.

[89] A. Katti *et al.*, "Chemical, physical, and mechanical characterization of isocyanate cross-Linked amine-modified silica aerogels," *Chem. Mater.*, 2006, doi: 10.1021/cm0513841.

[90] L. L. Hench and J. K. West, "The Sol-Gel Process," *Chem. Rev.*, 1990, doi: 10.1021/cr00099a003.

[91] R. P. Patel, N. S. Purohit, and A. M. Suthar, "An overview of silica aerogels," *International Journal of ChemTech Research*. 2009.

[92] A. Buzykaev *et al.*, "Aerogels with high optical parameters for Cherenkov counters," *Nucl. Instruments Methods Phys. Res. Sect. A Accel. Spectrometers, Detect. Assoc. Equip.*, 1996, doi: 10.1016/0168-9002(96)00571-2.

[93] M. Rubin and C. M. Lampert, "Transparent silica aerogels for window insulation," *Sol. Energy Mater.*, 1983, doi: 10.1016/0165-1633(83)90012-6.

[94] Q. Zhu, Y. Li, and Z. Qiu, "Research progress on aerogels as transparent insulation materials," in *Challenges on Power Engineering and Environment - Proceedings of the International Conference on Power Engineering 2007, ICOPE 2007*, 2007, doi: 10.1007/978-3-540-76694-0_207.

[95] G. M. Pajonk, "Aerogel catalysts," *Applied Catalysis*. 1991, doi: 10.1016/0166-9834(91)85054-Y.

[96] M. R. Ayers and A. J. Hunt, "Molecular oxygen sensors based on photoluminescent silica aerogels," *J. Non. Cryst. Solids*, 1998, doi: 10.1016/S0022-3093(98)00051-9.

[97] R. W. Pekala, "Organic aerogels from the polycondensation of resorcinol with formaldehyde," *J. Mater. Sci.*, 1989, doi: 10.1007/BF01139044.

[98] R. W. Pekala, C. T. Alviso, F. M. Kong, and S. S. Hulsey, "Aerogels derived from multifunctional organic monomers," *J. Non. Cryst. Solids*, 1992, doi: 10.1016/S0022-3093(05)80436-3.

[99] S. A. Al-Muhtaseb and J. A. Ritter, "Preparation and properties of resorcinol-formaldehyde organic and carbon gels," *Advanced Materials*. 2003, doi: 10.1002/adma.200390020.

[100] C. Lin, "Correlation of Double-Layer Capacitance with the Pore Structure of Sol-Gel Derived Carbon Xerogels," *J. Electrochem. Soc.*, 1999, doi: 10.1149/1.1392526.

[101] F. Rodríguez-Reinoso, “The role of carbon materials in heterogeneous catalysis,” *Carbon N. Y.*, 1998, doi: 10.1016/S0008-6223(97)00173-5.

[102] S. T. Mayer, “The Aerocapacitor: An Electrochemical Double-Layer Energy-Storage Device,” *J. Electrochem. Soc.*, 1993, doi: 10.1149/1.2221066.

[103] S. Haji and C. Erkey, “Removal of Dibenzothiophene from Model Diesel by Adsorption on Carbon Aerogels for Fuel Cell Applications,” *Ind. Eng. Chem. Res.*, 2003, doi: 10.1021/ie030518m.

[104] Y. Xu, K. Sheng, C. Li, and G. Shi, “Self-assembled graphene hydrogel via a one-step hydrothermal process,” *ACS Nano*, 2010, doi: 10.1021/nn101187z.

[105] K. Hu, X. Xie, M. Cerruti, and T. Szkopek, “Controlling the shell formation in hydrothermally reduced graphene hydrogel,” *Langmuir*, 2015, doi: 10.1021/acs.langmuir.5b00508.

[106] K. Hu, X. Xie, T. Szkopek, and M. Cerruti, “Understanding Hydrothermally Reduced Graphene Oxide Hydrogels: From Reaction Products to Hydrogel Properties,” *Chem. Mater.*, 2016, doi: 10.1021/acs.chemmater.5b04713.

[107] Y. Cheng *et al.*, “Enhanced mechanical, thermal, and electric properties of graphene aerogels via supercritical ethanol drying and high-Temperature thermal reduction,” *Sci. Rep.*, 2017, doi: 10.1038/s41598-017-01601-x.

[108] C. A. García-González, M. C. Camino-Rey, M. Alnaief, C. Zetzl, and I. Smirnova, “Supercritical drying of aerogels using CO 2: Effect of extraction time on the end material textural properties,” *J. Supercrit. Fluids*, 2012, doi: 10.1016/j.supflu.2012.02.026.

[109] “Handbook of Sol-Gel Science and Technology: Processing, Characterization and Applications, Volumes I−III Set edited by Sumio Sakka (Professor Emeritus of Kyoto University). Kluwer Academic Publishers: Boston, Dordrecht, London. 2005. lx + 1980 pp. $1500,” *J. Am. Chem. Soc.*, 2005, doi: 10.1021/ja041056m.

[110] C. Agustín-Sáenz, J. Á. Sánchez-García, M. Machado, M. Brizuela, O. Zubillaga, and A. Tercjak, “Broadband antireflective coating stack based on mesoporous silica by acid-catalyzed sol-gel method for concentrated photovoltaic application,” *Sol. Energy Mater. Sol. Cells*, 2018, doi: 10.1016/j.solmat.2018.06.040.

[111] “Sol-gel materials: chemistry and applications,” *Choice Rev. Online*, 2001, doi: 10.5860/choice.38-6197.

[112] S. Esposito, "'Traditional' sol-gel chemistry as a powerful tool for the preparation of supported metal and metal oxide catalysts," *Materials*. 2019, doi: 10.3390/ma12040668.

[113] A. P. Rao, A. V. Rao, and G. M. Pajonk, "Hydrophobic and physical properties of the two step processed ambient pressure dried silica aerogels with various exchanging solvents," *J. Sol-Gel Sci. Technol.*, 2005, doi: 10.1007/s10971-005-4662-1.

[114] A. Witkowski, M. Majkut, and S. Rulik, "Analysis of pipeline transportation systems for carbon dioxide sequestration," *Arch. Thermodyn.*, 2014, doi: 10.2478/aoter-2014-0008.

[115] R. Baetens, B. P. Jelle, and A. Gustavsen, "Aerogel insulation for building applications: A state-of-the-art review," *Energy and Buildings*. 2011, doi: 10.1016/j.enbuild.2010.12.012.

[116] H. Maleki, "Recent advances in aerogels for environmental remediation applications: A review," *Chemical Engineering Journal*. 2016, doi: 10.1016/j.cej.2016.04.098.

[117] O. Ergen, E. Celik, A. H. Unal, M. Y. Erdolu, F. E. Oztuna Sarac, and U. Unal, "Real Time Chemical and Mechanical Human Motion Monitoring with Aerogel Based Wearable Sensors," *R. Soc. Chem.*, 2020.

[118] J. Stergar and U. Maver, "Review of aerogel-based materials in biomedical applications," *Journal of Sol-Gel Science and Technology*. 2016, doi: 10.1007/s10971-016-3968-5.

[119] M. Amjadi, K. U. Kyung, I. Park, and M. Sitti, "Stretchable, Skin-Mountable, and Wearable Strain Sensors and Their Potential Applications: A Review," *Advanced Functional Materials*. 2016, doi: 10.1002/adfm.201504755.

[120] H. Liu *et al.*, "Electrically conductive polymer composites for smart flexible strain sensors: a critical review," *Journal of Materials Chemistry C*. 2018, doi: 10.1039/C8TC04079F.

[121] J. Zhou *et al.*, "Flexible piezotronic strain sensor," *Nano Lett.*, 2008, doi: 10.1021/nl802367t.

[122] W. Zhang, R. Zhu, V. Nguyen, and R. Yang, "Highly sensitive and flexible strain sensors based on vertical zinc oxide nanowire arrays," *Sensors Actuators, A Phys.*, 2014, doi: 10.1016/j.sna.2013.11.004.

[123] X. Xiao *et al.*, “High-strain sensors based on ZnO nanowire/polystyrene hybridized flexible films,” *Adv. Mater.*, 2011, doi: 10.1002/adma.201103406.

[124] Q. Chen, Y. Sun, Y. Wang, H. Cheng, and Q. M. Wang, “ZnO nanowires-polyimide nanocomposite piezoresistive strain sensor,” *Sensors Actuators, A Phys.*, 2013, doi: 10.1016/j.sna.2012.11.006.

[125] Q. Liao, M. Mohr, X. Zhang, Z. Zhang, Y. Zhang, and H. J. Fecht, “Carbon fiber-ZnO nanowire hybrid structures for flexible and adaptable strain sensors,” *Nanoscale*, 2013, doi: 10.1039/c3nr03536k.

[126] H. Gullapalli *et al.*, “Flexible piezoelectric zno-paper nanocomposite strain sensor,” *Small*, 2010, doi: 10.1002/smll.201000254.

[127] S. K. Sharma, A. Rammohan, and A. Sharma, “Templated one step electrodeposition of high aspect ratio n-type ZnO nanowire arrays,” *J. Colloid Interface Sci.*, 2010, doi: 10.1016/j.jcis.2009.12.026.

[128] M. Babucci *et al.*, “Atomically dispersed reduced graphene aerogel-supported iridium catalyst with an iridium loading of 14.8 wt %,” *ACS Catal.*, 2019, doi: 10.1021/acscatal.9b02231.

[129] D. J. Lipomi *et al.*, “Skin-like pressure and strain sensors based on transparent elastic films of carbon nanotubes,” *Nat. Nanotechnol.*, 2011, doi: 10.1038/nnano.2011.184.

[130] H. O. Pierson, *Handbook of chemical vapor deposition (CVD)*. 1999.

[131] *Introductory Raman Spectroscopy*. 1994.

[132] A. A. Bunaciu, E. gabriela Udriştioiu, and H. Y. Aboul-Enein, “X-Ray Diffraction: Instrumentation and Applications,” *Critical Reviews in Analytical Chemistry*. 2015, doi: 10.1080/10408347.2014.949616.

[133] G.-J. Janssen, “Information on the FESEM (Field-emission Scanning Electron Microscope),” *Radboud Univ. Nijmegen*, 2015.

[134] Y. Q. Li, P. Huang, W. Bin Zhu, S. Y. Fu, N. Hu, and K. Liao, “Flexible wire-shaped strain sensor from cotton thread for human health and motion detection,” *Sci. Rep.*, 2017, doi: 10.1038/srep45013.

[135] S. T. Nguyen, H. T. Nguyen, A. Rinaldi, N. P. V. Nguyen, Z. Fan, and H. M. Duong, “Morphology control and thermal stability of binderless-graphene aerogels from graphite for energy storage applications,” *Colloids Surfaces A Physicochem. Eng. Asp.*, 2012, doi: 10.1016/j.colsurfa.2012.08.048.

[136] L. Zhang, G. Chen, M. N. Hedhili, H. Zhang, and P. Wang, “Three-dimensional assemblies of graphene prepared by a novel chemical reduction-induced self-assembly method,” *Nanoscale*, 2012, doi: 10.1039/c2nr32157b.

[137] I. Kondratowicz, K. Zelechowska, D. Majdecka, and R. Bilewicz, “Synthesis and modification of reduced graphene oxide aerogels for biofuel cell applications,” *Mater. Sci. Pol.*, 2015, doi: 10.1515/msp-2015-0042.

[138] Y. A. Eren Z.S., Gezer G., Tuncer S., Yildirim L.T., Banerjee S., “Improved Solubility of Celecoxib by Inclusion in SBA-15 Mesoporous Silica: Drug Loading in Different Solvents and Release,” *Microporous Mesoporous Mater.*, vol. 235, pp. 211–223, 2016.

[139] X. Wu *et al.*, “High-rate capacitive performance of graphene aerogel with a superhigh C/O molar ratio,” *J. Mater. Chem.*, 2012, doi: 10.1039/c2jm35278h.

[140] E. García-Bordejé, S. Víctor-Román, O. Sanahuja-Parejo, A. M. Benito, and W. K. Maser, “Control of the microstructure and surface chemistry of graphene aerogels: Via pH and time manipulation by a hydrothermal method,” *Nanoscale*, 2018, doi: 10.1039/c7nr08732b.

[141] Y. W. Heo *et al.*, “ZnO nanowire growth and devices,” *Materials Science and Engineering R: Reports*. 2004, doi: 10.1016/j.mser.2004.09.001.

[142] S. O. Kucheyev, J. E. Bradby, J. S. Williams, C. Jagadish, and M. V. Swain, “Mechanical deformation of single-crystal ZnO,” *Appl. Phys. Lett.*, 2002, doi: 10.1063/1.1448175.

[143] S. Y. Ting *et al.*, “Crystallinity improvement of ZnO thin film on different buffer layers grown by MBE,” *J. Nanomater.*, 2012, doi: 10.1155/2012/929278.

[144] J. Mao *et al.*, “Physics of Semiconductor Devices,” *Sensors Actuators, A Phys.*, 2012, doi: 10.1088/0957-4484/23/7/075402.

[145] J. Zhou *et al.*, “Piezoelectric-potential-controlled polarity-reversible Schottky diodes and switches of ZnO wires,” *Nano Lett.*, 2008, doi: 10.1021/nl802497e.

[146] J. Yoon, F. Huang, K. H. Shin, J. I. Sohn, and W. K. Hong, “Effects of applied voltages on the charge transport properties in a ZnO nanowire field effect transistor,” *Materials (Basel).*, 2020, doi: 10.3390/ma13020268.

[147] S. Wu *et al.*, “Strain Sensors with Adjustable Sensitivity by Tailoring the Microstructure of Graphene Aerogel/PDMS Nanocomposites,” *ACS Appl. Mater. Interfaces*, 2016, doi: 10.1021/acsami.6b06012.

[148] J. Jia, X. Sun, X. Lin, X. Shen, Y. W. Mai, and J. K. Kim, “Exceptional electrical conductivity and fracture resistance of 3D interconnected graphene foam/epoxy composites,” *ACS Nano*, 2014, doi: 10.1021/nn500590g.

[149] Z. Wang *et al.*, “Graphene aerogel/epoxy composites with exceptional anisotropic structure and properties,” *ACS Appl. Mater. Interfaces*, 2015, doi: 10.1021/acsami.5b00146.

[150] S. Nardecchia, D. Carriazo, M. L. Ferrer, M. C. Gutiérrez, and F. Del Monte, “Three dimensional macroporous architectures and aerogels built of carbon nanotubes and/or graphene: Synthesis and applications,” *Chem. Soc. Rev.*, 2013, doi: 10.1039/c2cs35353a.

LIST OF PUBLICATIONS

[1] O. Ergen, **E. Celik**, A. H. Unal, M. Y. Erdolu, F. E. Sarac, and U. Unal, "Real Time Chemical and Mechanical Human Motion Monitoring with Aerogel Based Wearable Sensors," *Lab Chip,* 2020, doi: 10.1039/d0lc00545b.

[2] O. Ergen, **E. Celik**, A. H. Unal, and M. Y. Erdolu, "Screen Engineered Field Effect CuO Based Solar Cells," *IEEE Electron Device Lett.,* 2020, doi: 10.1109/LED.2020.2995924.